TITLE:

# Phospholipid‐flipping activity of P4‐ATPase drives membrane curvature

AUTHOR(S):

Takada, Naoto; Naito, Tomoki; Inoue, Takanari; Nakayama, Kazuhisa; Takatsu, Hiroyuki; Shin, Hye‐Won

1 **Phospholipid-flipping activity of P4-ATPase drives membrane curvature**

2 Naoto Takada[1], Tomoki Naito[1], Takanari Inoue[2], Kazuhisa Nakayama[1], Hiroyuki Takatsu[1],

3 and Hye-Won Shin[1][*]

4 [1]Graduate School of Pharmaceutical Sciences, Kyoto University, Sakyo-ku, Kyoto 606-8501,

5 Japan; [2]Department of Cell Biology, Center for Cell Dynamics, Johns Hopkins University

6 School of Medicine, Baltimore, MD21205

7 [*]To whom correspondence should be addressed: Hye-Won Shin, Graduate School of

8 Pharmaceutical Sciences, Kyoto University, Sakyo-ku, Kyoto 606-8501, Japan; Tel: +81-75-

9 753-4537; Fax: +81-75-753-4557; E-mail: shin@pharm.kyoto-u.ac.jp

10

11 Running title: P4-ATPases drive membrane curvature

12

13 Keywords: plasma membrane, lipid, flippase, BAR domain, curvature

14

15 **Abstract**

16    P4-ATPases are phospholipid flippases that translocate phospholipids from the

17 exoplasmic/luminal to the cytoplasmic leaflet of biological membranes. All P4-ATPases in

18 yeast and some in other organisms are required for membrane trafficking; therefore, changes

19 in the transbilayer lipid composition induced by flippases are thought to be crucial for

20 membrane deformation. However, it is poorly understood whether the phospholipid-flipping

21 activity of P4-ATPases can promote membrane deformation. In this study, we assessed

22 membrane deformation induced by flippase activity via monitoring the extent of membrane

23 tubulation using a system that allows inducible recruitment of Bin/Amphiphysin/RVS (BAR)

24 domains to the plasma membrane (PM). Enhanced phosphatidylcholine-flippase activity at the

25 PM due to expression of ATP10A, a member of the P4-ATPase family, promoted membrane

26 tubulation upon recruitment of BAR domains to the PM. This is the important evidence that

27 changes in the transbilayer lipid composition induced by P4-ATPases can deform biological

28 membranes.

29

30 **Introduction**

31    P4-ATPases flip phospholipids across the bilayer to generate and regulate the

32 asymmetric distributions of lipids in eukaryotic cells. Phosphatidylserine (PS) and

33 phosphatidylethanolamine (PE) are enriched in the cytoplasmic leaflet of the plasma membrane

34 (PM), whereas phosphatidylcholine (PC) and sphingomyelin are abundant in the exoplasmic

35 leaflet (Devaux, 1991, Murate *et al.*, 2015, Zachowski, 1993). Genetic studies in

36 *Saccharomyces cerevisiae*, *Arabidopsis thaliana*, and *Caenorhabditis elegans* revealed that

37 P4-ATPases play roles in membrane trafficking. All five yeast P4-ATPases are involved in

38 membrane trafficking at different stages of the secretory and endocytic pathways (Graham &

39 Burd, 2011, Muthusamy *et al.*, 2009). In addition, PS flipping at the *trans*-Golgi network

40 participates in exocytic protein sorting and enhances membrane curvature in yeast (Chen *et al.*,

41 1999, Hankins *et al.*, 2015, Xu *et al.*, 2013). The human genome encodes 14 P4-ATPases;

42 however, their functions are poorly understood (Andersen *et al.*, 2016). Among mammalian

43 P4-ATPases, ATP8A1 and ATP9A are required for endosome-mediated membrane trafficking,

44 and PS flipping by ATP8A1 is needed for recruitment of EHD1 to recycling endosomes (Lee

45 *et al.*, 2015, Tanaka *et al.*, 2016). Therefore, the activities of P4-ATPases seem to be required

46 for the recruitment of proteins involved in membrane trafficking to cellular compartments.

47 Another plausible hypothesis is that P4-ATPase–mediated phospholipid translocation

48 generates an imbalance in the level of lipids between the leaflets of the bilayer. The resultant

49 lipid-loading in the cytoplasmic leaflet would drive inwardly directed membrane deformation,

50 leading to the membrane curvature required for vesicle budding (Graham, 2004, Panatala *et al.*,

51 2015, Takeda *et al.*, 2014). Cell shape drastically changes upon exogenous application of lyso-

52 PC or impermeable amphipathic drugs, suggesting that the shape of lipid species and/or an

53 imbalance in lipid mass (translocation of lyso-PC is much slower than that of PC) are involved

54 in the generation of membrane curvature (Devaux *et al.*, 2008, Sheetz & Singer, 1974).

55 Changes in lipid composition following addition of exogenous phospholipids alter the shape

56 of erythrocytes, and it was thus hypothesized that ATP-dependent lipid translocases at the PM

57 are involved in membrane shape changes (Daleke & Huestis, 1989, Seigneuret & Devaux,

58 1984). We and other groups have recently shown the flippase activities of mammalian P4-

59 ATPases (Lee *et al.*, 2015, Naito *et al.*, 2015, Segawa *et al.*, 2016, Takatsu *et al.*, 2014, Zhu *et*

60 *al.*, 2012) using a cell-based flippase assay. However, it remains unknown whether flippase

61 activity of P4-ATPase family can induce membrane curvature because spatiotemporal flippase

62 activity cannot be visualized together with membrane deformation in biological membranes.

63 To overcome this technical problem, we designed an experiment to indirectly assess membrane

64 deformation induced by flippase activity in the PM.

65      We have previously shown that enhanced PC-flippase activity at the PM changes cell

66 shape, decreases cell size, and delays cell spreading on extracellular matrix, possibly by

67 increasing inwardly directed PM bending (Miyano *et al.*, 2016, Naito *et al.*, 2015). Therefore,

68    spatiotemporally regulated movement of lipids between the leaflets of the bilayer could

69    contribute to PM remodeling. In fact, a mutation in the mouse *ATP11C* gene, another member

70    of the P4-ATPase family, alters the morphology of erythrocytes (Yabas *et al.*, 2014), and a

71    complex comprising ATP8A1 and CDC50A has been implicated to play a role in cell migration

72    (Kato *et al.*, 2013). CDC50A interacts with most P4-ATPases and is required for the transport

73    of newly synthesized P4-ATPases from the endoplasmic reticulum to cellular compartments

74    and/or the PM (Naito *et al.*, 2015, Takatsu *et al.*, 2011).

75         To investigate whether a lipid imbalance in the bilayer induced by P4-ATPases is

76    directly linked with membrane curvature, we used BIN/Amphiphysin/Rvs (BAR) domains,

77    which dimerize to form a crescent-shaped structure, sense membrane curvature, and generate

78    tubular membrane structures via self-oligomerizing in biological membranes (Frost *et al.*, 2008,

79    Itoh & De Camilli, 2006, Peter *et al.*, 2004, Yin *et al.*, 2009). BAR domains are categorized

80    into four main subfamilies: classic BAR, N-terminal amphipathic helix-containing BAR (N-

81    BAR), Fes-CIP4 homology BAR (F-BAR), and inverse BAR (I-BAR) (Frost *et al.*, 2009, Itoh

82    & De Camilli, 2006). These domains mediate membrane curvature by performing scaffolding

83    roles and/or inserting amphipathic helices along lipid bilayers, and form membrane tubules in

84    cells and artificial liposomes (Bhatia *et al.*, 2009, Gallop *et al.*, 2006, Masuda *et al.*, 2006,

85    Poudel *et al.*, 2016).

86         Membrane deformation/tubulation induced by BAR domains from the PM has been

87    visualized using a chemically inducible dimerization (CID) technique that allows acute

88    recruitment of these domains to the PM (Komatsu *et al.*, 2010, Suarez *et al.*, 2014). The PM-

89    recruited N-BAR domain induces dramatic membrane tubulation from the PM (Suarez *et al.*,

90    2014). By striking contrast, the ΔN-BAR domain, which lacks the N-terminal amphipathic

91    helix of the N-BAR domain and thus is structurally similar to classic BAR domains, and the F-

92    BAR domain rarely promote the formation of membrane tubules from the PM (Suarez *et al.*,

93    2014), although classic BAR and F-BAR domains can induce membrane tubule formation from

94    liposomes (Henne *et al.*, 2007, Peter *et al.*, 2004). The amphipathic helix of the N-BAR domain

95    penetrates the lipid bilayer, leading to increased membrane curvature into the cytoplasm, and

96    the BAR domain subsequently senses this curvature and drives membrane tubule formation

97    (Figure 8A) (Campelo *et al.*, 2008, Gallop *et al.*, 2006, McMahon & Boucrot, 2015, Poudel *et

98    al.*, 2016). Therefore, we hypothesized that if proper membrane curvature is generated, the ΔN-

99    BAR and/or F-BAR domains should be able to induce the generation of membrane tubules

100   from the PM in the same way as the N-BAR domain does. We assessed membrane curvature

3

101 induced by flippase activity via monitoring the extent of membrane tubulation using the CID

102 technique that allows acute recruitment of BAR domains to the PM.

103

104 **Results and Discussion**

105 ***Recruitment of the N-BAR domain, but not of the ΔN-BAR or F-BAR domain, to the PM***

106 ***induces the generation of membrane tubules from the PM.***

107       We transfected HeLa cells with two constructs: fluorescent protein-fused PM-targeting

108 FRB [FK506-binding protein (FKBP)-rapamycin-binding domain] and fluorescent protein-

109 fused FKBP-BAR domains (Figure EV1A). TagBFP2- or TagRFP-tagged FRB was targeted

110 to the PM by adding the N-terminal 11 amino acids (a.a.) of Lyn, and EGFP- or mCherry-

111 tagged FKBP was fused to each BAR domain [N-BAR (N-BAR domain of human amphiphysin

112 1), ΔN-BAR (lacking the N-terminal amphipathic helix of the N-BAR domain), or F-BAR (F-

113 BAR domain of formin-binding protein 17, FBP17)] (Suarez *et al.*, 2014). The morphology of

114 the PM was visualized by confocal or epifluorescence microscopy, as shown by fluorescent

115 signals of the PM-targeting FRB and FKBP-BAR domains, following treatment with

116 rapamycin, which triggers heterodimerization of FRB and FKBP (Figure EV1A). In the

117 absence of rapamycin, all FKBP-BAR domains, as well as EGFP-FKBP, were predominantly

118 distributed throughout the cytoplasm, and PM-targeting FRB was localized at the PM as

119 described previously (Figure EV1B–D, a and c, Movies EV1–EV4) (Suarez *et al.*, 2014). Upon

120 treatment with rapamycin, the FKBP-BAR domains and EGFP-FKBP were rapidly recruited

121 to the PM (Figure EV1B–D, b–b'' and d–d'', Movies EV1–EV4). The CID-engineered N-BAR

122 domain rapidly induced dramatic formation of tubular structures from the PM (Figure EV1B

123 b–b'' and d–d'', Movie EV2, Figure 8) (Suarez *et al.*, 2014, Yin *et al.*, 2009). These tubular

124 structures did not colocalize with markers of endosomes or the Golgi complex (Figure EV1E);

125 therefore, it is unlikely that they were generated from these intracellular compartments. By

126 contrast, the CID-engineered ΔN-BAR and F-BAR domains, as well as EGFP alone, failed to

127 induce membrane tubulation from the PM, even if they were efficiently recruited to the PM

128 upon rapamycin treatment (Figure EV1C and D, b–b'' and d–d'', Movies EV1, EV3, and EV4)

129 (Suarez *et al.*, 2014). Thus, penetration of the amphipathic helix of the N-BAR domain may

130 have a wedging effect, leading to increased curvature of the PM into the cytoplasm, and the

131 BAR domain may subsequently sense this membrane curvature and drive membrane tubulation

132 via oligomerizing along the membrane (Figure 8A) (Campelo *et al.*, 2008, Gallop *et al.*, 2006,

133 Poudel *et al.*, 2016).

4

134

***Recruitment of the ΔN-BAR or F-BAR domain to the PM leads to the generation of***

***membrane tubules in cells stably expressing ATP10A***

We previously showed that ATP10A localizes at the PM and exhibits relatively high PC-flipping activity, and that its exogenous expression changes cell shape and delays cell adhesion and cell spreading on the extracellular matrix (Miyano *et al.*, 2016, Naito *et al.*, 2015). PC is primarily enriched in the exoplasmic leaflet of the PM (Murate *et al.*, 2015). Thus, increased PC-flippase activity due to ATP10A expression allows continuous and excessive phospholipid flipping from the exoplasmic to the cytoplasmic leaflet, resulting in changes in cell shape, decreases in cell size, and delays in cell spreading (Miyano *et al.*, 2016, Naito *et al.*, 2015). ATP10A is not expressed in HeLa cells (Takatsu *et al.*, 2011) (Figure EV4A), and thus its expression may have marked effects on these cells. We hypothesized that ATP10A expression might trigger inward bending of the PM, thereby promoting membrane tubulation induced by PM-recruited BAR domains. To test this hypothesis, we used HeLa cells stably expressing ATP10A; the ATP10A(E203Q) mutant, which lacks ATPase activity; and ATP11A, which specifically flips PS/PE at the PM (Takatsu *et al.*, 2014) (Figure 1). The expression level of ATP10A was comparable to that of ATP10A(E203Q) and lower than that of ATP11A (Figure EV2A), and PC-flippase activity was not altered upon rapamycin treatment (Figure EV2B). We also confirmed that the PC-flippase activity of ATP10A was not altered upon expression of BAR domains or their recruitment to the PM (Figure EV2C).

Recruitment of the ΔN-BAR or F-BAR domain to the PM did not cause membrane tubulation in parental HeLa cells (Figures EV1C and D). By contrast, recruitment of the ΔN-BAR or F-BAR domain to the PM induced drastic membrane tubulation in cells expressing ATP10A (Figure 1A and D, b, b', d, and d', Movies EV5, EV6, EV9, and EV10), but not in cells expressing ATP10A(E203Q) (Figure 1B and E, b, b', d, and d', Movie EV7). These results demonstrate that the PC-flippase activity of ATP10A mediates membrane tubule formation. Recruitment of the N-BAR domain to the PM caused membrane tubulation in parental HeLa cells as well as cells expressing ATP10A, ATP10A(E203Q), and ATP11A (Figure 1G-I, b' and d' and Figure EV1B). No tubular membrane structures were observed in cells not treated with rapamycin (Figure 1A, D, and G, a and c, Movies EV5 and EV6). For semi-quantitative analysis, we counted the numbers of cells containing tubular membrane structures following rapamycin treatment. Recruitment of the ΔN-BAR or F-BAR domain to the PM in ATP10A-expressing cells increased the proportion of cells containing tubular structures relative to

5

167    control and ATP10A(E203Q)-expressing cells (Figure 1J and K). Although the PM-recruited

168    N-BAR domain drove membrane tubulation in parental HeLa cells (Figure EV1B, Figure 1L

169    (-)), the number of cells containing tubular structures was slightly higher among those

170    expressing ATP10A, but not among those expressing ATP10A(E203Q) or ATP11A (Figure

171    1L).

172        The PM-recruited ΔN-BAR and F-BAR domains did not cause membrane tubulation in

173    cells expressing ATP11A, which flips PS/PE at the PM (Takatsu *et al.*, 2014) (Figure 1C and

174    F, b, b', d, and d'). The level of PS/PE is limited in the exoplasmic leaflet (Murate *et al.*, 2015,

175    Op den Kamp, 1979); therefore, exogenous expression of ATP11A may not trigger membrane

176    deformation. Therefore, excessive PC flipping from the outer to the inner leaflet driven by

177    ATP10A generates membrane curvature by inducing an imbalance of lipid mass between the

178    two leaflets.

179        Disruption of cytoskeleton leads to a reduction in membrane tension that can initiate

180    membrane tubulation mediated by an N-BAR domain-containing protein (Gauthier *et al.*, 2012,

181    Masters *et al.*, 2013, Shi & Baumgart, 2015). We therefore investigated whether this membrane

182    tubulation, which is induced by BAR domains in ATP10A-expressing cells, is caused by

183    disruption of cytoskeleton. The integrity of the actin cytoskeleton and microtubules was not

184    affected by expression of ATP10A or recruitment of the ΔN-BAR domain to the PM in

185    ATP10A-expressing cells in comparison with control cells (Figure 2A and B, a, a', d, d', g,

186    and g'). These results suggest that enhanced PC-flipping activity increases inward bending of

187    the PM and generates membrane curvature. Thus, the PM-recruited ΔN-BAR and F-BAR

188    domains stably interact with curved membranes, resulting in membrane tubulation from the

189    PM.

190

191    ***Disruption of microtubules attenuates membrane tubulation caused by BAR domains***

192        We next asked whether the membrane tubulation generated by the recruitment of BAR

193    domains to the PM is dependent on microtubules. To this end, we treated cells with nocodazole

194    to disrupt microtubules (Figure 3A–D, d). We confirmed that nocodazole treatment did not

195    affect the flippase activity of ATP10A (Figure EV2D). Nocodazole treatment reduced the

196    formation of tubular membrane structures by PM-recruited N-BAR domain (Figure 3A e–f',

197    and E). In addition, membrane tubules generated by PM-recruited ΔN-BAR or F-BAR domain

198    in ATP10A-expressing cells were also reduced by treatment with nocodazole (Figure 3C and

199    D, e–f', and F and G). Therefore, the membrane tubulation by the BAR-domains was in a

200　manner dependent on microtubules. Although cell populations containing long tubular

201　structures were reduced upon nocodazole treatment (Figure 3E–G), very short tubules were

202　observed (Figure 3A and C, e'' and f'') suggesting the possibility that elongation of membrane

203　tubules require the integrity of microtubules.

204

205　***An increase in PM tension prevents the generation of membrane tubules by BAR domains***

206　　　We next investigated whether inward bending of the PM is a prerequisite for membrane

207　tubulation driven by PM-recruited BAR domains. To this end, we examined whether an

208　increase in PM tension inhibited BAR domain-driven membrane tubulation by exposing cells

209　to hypotonic medium (Figures 4 and 5). Intriguingly, recruitment of the N-BAR domain to the

210　PM did not induce membrane tubulation in cells exposed to hypotonic conditions (Figure 4A

211　e–f' and E, Movies EV2 and EV8). Cells were exposed to hypotonic medium before or after

212　treatment with rapamycin (Movie EV8 and EV2, respectively) and cells did not generate

213　membrane tubules in either case. Upon exposure to hypotonic conditions, cells swelled acutely

214　(Movies EV2, EV5, and EV8), indicating that PM tension was increased. These results suggest

215　that outward swelling of cells negatively affects membrane curvature toward the cytoplasm.

216　We next investigated whether a decrease in membrane tension triggers membrane tubulation

217　by exposing cells to hypertonic medium. However, hypertonic stress did not significantly affect

218　membrane tubulation driven by the N-BAR domain (Figure 4B e–f' and F) or trigger membrane

219　tubulation driven by the ΔN-BAR domain (Figure 4D e–f' and G). Thus, even in shrunken cells

220　exposed to hypertonic medium, the PM may not bend properly to allow the ΔN-BAR domain

221　to form membrane tubules.

222　　　Exposure to hypotonic medium also abrogated membrane tubulation induced by the PM-

223　recruited ΔN-BAR and F-BAR domains in ATP10A-expressing cells (Figure 5A and C, e–f',

224　E, F, Movie EV5). Membrane tubules induced by the PM-recruited ΔN-BAR domain was

225　readily disappeared upon exposure to hypotonic medium (Movie EV5), suggesting that tubular

226　structures are highly dynamic and susceptible to a change in membrane tension. Thus, outward

227　swelling of cells prevents inward PM bending triggered by the flippase activity of ATP10A

228　and by insertion of the amphipathic helix of the N-BAR domain. Notably, the PC-flippase

229　activity of ATP10A was abrogated under hypotonic conditions (Figure EV2D). Therefore, we

230　cannot exclude the possibility that ablation of membrane tubules upon hypotonic stress is

231　associated with the lack of flippase activities. However, we think that the disappearance of

232　membrane tubules under hypotonic condition is due to the increase in membrane tension which

7

233  prevents inward PM bending, because the N-BAR domain did not generate membrane tubules

234  (Figure 4A). Exposure to hypertonic medium did not affect membrane tubulation driven by the

235  ΔN-BAR or F-BAR domain in ATP10A-expressing cells (Figure 5B and D, e–f'). This result

236  corresponds to the membrane tubulation driven by the N-BAR domain (Figure 4B and F).

237  Membrane tubulation was not observed in ATP10A(E203Q)-expressing cells under any

238  condition (Figure EV3).

239

240  ***Depletion of ATP10A inhibits membrane tubulation induced by the ΔN-BAR and F-BAR***

241  ***domains in cells stably expressing exogenous ATP10A***

242  To confirm that the flippase activity of ATP10A is indispensable for deformation of the

243  PM, we knocked down ATP10A via RNAi in cells stably expressing this flippase. Efficient

244  knockdown of ATP10A was confirmed by immunoblot analysis (Figure EV4B), measurement

245  of PC-flippase activity (Figure EV4C), and immunofluorescence analysis (Figure 6A, C, and

246  E, k and l). Membrane tubulation driven by recruitment of the ΔN-BAR and F-BAR domains

247  to the PM was significantly decreased in ATP10A-depleted cells (Figure 6A and C, h, h', j,

248  and j', B, and D). These results revealed that membrane tubulation induced by the ΔN-BAR

249  and F-BAR domains in ATP10A-expressing cells is due to increased PC-flippase activity at

250  the PM. Membrane tubulation induced by the N-BAR domain was not decreased in ATP10A-

251  depleted cells (Figure 6E h, h', j, and j', and F), probably due to its high membrane-deforming

252  activity and/or a modest level of residual ATP10A protein (Figure EV4B).

253

254  ***Enhanced PC-flipping activity increases endocytosis of β1-integrin***

255  Since incubation with phospholipids, but not lyso-phospholipids, enhances endocytosis in

256  K562 cells (Farge *et al.*, 1999), it was hypothesized that phospholipid treatment increased the

257  concentration of phospholipids in the inner leaflet of the PM and endocytosis was subsequently

258  enhanced. We examined whether increased flippase activity upon ATP10A expression

259  facilitates endocytosis. To this end, β1-integrin internalization was examined by following an

260  extracellularly applied anti-β1-integrin antibody (Figure 7A). Cells were incubated with an

261  anti-β1-integrin antibody at 4°C for 1 h, washed with ice-cold PBS to remove unbound

262  antibodies, and incubated at 37°C for the indicated durations to allow the internalization of β1-

263  integrin (Figure 7). Cells were then washed with acidic solution to remove residual antibodies

264  on the PM. The fluorescence intensity of intracellular β1-integrin was estimated in cells

265  expressing ATP10A and ATP10A(E203Q) and parental cells. Internalization of β1-integrin

8

266  was significantly increased at 15 and 30 min in cells stably expressing ATP10A, but not in

267  those stably expressing ATP10A(E203Q) (Figure 7B). In addition, the internalization was not

268  altered in cells stably expressing ATP11A as compared with control cells (Figure 7B). As we

269  discussed above, the level of PS/PE is limited in the exoplasmic leaflet (Murate *et al.*, 2015,

270  Op den Kamp, 1979); therefore, exogenous expression of ATP11A may not trigger the

271  phospholipids imbalance and membrane deformation. Therefore, enhanced inward bending of

272  the PM induced by ATP10A expression facilitates the internalization of β1-integrin, which

273  may delay cell adhesion and cell spreading on extracellular matrix (Miyano *et al.*, 2016, Naito

274  *et al.*, 2015). We also recognized that ATP1A1 (Na/K pump), which mainly localizes to the

275  PM, appeared more frequently in intracellular puncta in cells expressing ATP10A than in

276  control cells (Figure EV5A). Counting of cells in which ATP1A1 localized to the PM, and the

277  PM and cellular puncta revealed that intracellular ATP1A1 was substantially increased in cells

278  expressing ATP10A but not ATP10A(E203Q) (Figure EV5B) suggesting that ATP10A

279  expression increased the internalization of ATP1A1.

280      Then we asked whether depletion of endogenous ATP10A affects the β1-integrin

281  endocytosis. To this end, we depleted ATP10A by CRSIPR/Cas9 system in MDA-MB-231

282  cells which express endogenous ATP10A (Figures EV4A, and EV6A and B) and examined the

283  β1-integrin internalization in the knockout cells. As shown in Figure EV6, although knockout

284  of endogenous ATP10A tended to decrease the endocytosis of β1-integrin, the decrease was

285  not statistically significant (Figure EV6C). One possibility would be a functional redundancy

286  of other PC-flippases because MDA-MB-231 cells express PC-flippases such as ATP8B1 and

287  ATP8B2 (Takatsu *et al.*, 2014) (Figure EV6D).

288      Taken together, these results strongly suggest that enhancement of PC-flipping in

289  ATP10A-expressing cells induces an imbalance in the level of lipids between the leaflets of

290  the bilayer and increases inward PM bending, driving membrane curvature and allowing

291  membrane tubulation by BAR domains, even those that lack the N-terminal amphipathic helix.

292  Given that an increase in PM tension following hypotonic treatment suppressed membrane

293  tubulation driven by the N-BAR domain in parental HeLa cells, as well as by the ΔN-BAR and

294  F-BAR domains in ATP10A-expressing cells, membrane curvature induced by the N-terminal

295  amphipathic helix of N-BAR or enhanced PC-flippase activity (Figure 8A and B) is a

296  prerequisite for membrane tubulation. PC is abundant in the outer leaflet of the PM; therefore,

297  enhanced PC flipping by ATP10A most likely causes a lipid imbalance. On the other hand,

298  PS/PE is confined to the inner leaflet of the PM, meaning that expression of ATP11A may not

299    generate a lipid imbalance to allow membrane deformation. Notably, phospholipid flipping at

300    the PM was generally suppressed in hypotonic conditions but not in hypertonic conditions

301    (Figure EV2D). This suggests that an acute increase in membrane tension inhibits not only

302    membrane bending but also transbilayer lipid translocation.

303        In yeast, inactivation of Drs2p, a Golgi-localized PS-flippase, inhibits recruitment of Arf-

304    GTPase-activating protein (Gcs1p) to Golgi and endosomal membranes. Gcs1p contains an

305    amphipathic, α-helical ArfGAP lipid packing sensor (ALPS) motif, which plays a critical role

306    in recruitment of Gcs1p to membranes by sensing membrane curvature. Therefore, the PS-

307    flippase activity of Drs2p may be required to generate membrane curvature, which allows the

308    recruitment of Gcs1p to membranes (Xu *et al.*, 2013). Indeed, yeast cells depleted of Drs2p

309    accumulated aberrant membrane structures (Chen *et al.*, 1999). There are other explanations

310    for these observations, such as an electrostatic interaction between Gcs1p and PS. While this

311    study provides evidence for an effect of transbilayer lipid-mass changes on membrane

312    deformation since electrostatic effects on the PM can be excluded because PC is a neutral

313    phospholipid. In addition, phospholipid flipping itself, regardless of which phospholipid is

314    flipped, seems to be required for vesicle formation in yeast (Takeda *et al.*, 2014). Together with

315    our findings, phospholipid-flipping activities of P4-ATPases are able to induce membrane

316    curvature by generating an imbalance in the level of lipids between the two leaflets of the PM

317    and other cellular compartments, regardless of the flipped phospholipid species. The data

318    presented herein provide the important experimental evidence that phospholipid-flippase

319    activity can deform biological membranes. This raises questions when, where, and how

320    flippases can act. We recently have revealed the signal-dependent regulation mechanism of

321    ATP11C, a PS-flippase (Takatsu *et al.*, 2017). Elucidation of regulation mechanisms of P4-

322    ATPases including PC-flippases enable understanding of how P4-ATPases play roles in many

323    cellular processes involving membrane deformation, including membrane trafficking and cell

324    migration.

325

326    **Materials and Methods**

327    *Plasmids*

328        Constructs for C-terminally HA-tagged P4-ATPases were generated as described

329    previously (Takatsu *et al.*, 2011, Takatsu *et al.*, 2014). Constructs for FKBP-conjugated

330    fluorescent N-BAR (human amphiphysin 1, a.a. 1–248), ΔN-BAR (a.a. 26–248), F-BAR

331    (human FBP17, a.a. 1–300), and FRB-conjugated Lyn (a.a. 1–11) were obtained as described

previously (Komatsu *et al.*, 2010, Suarez *et al.*, 2014). DNA fragments of Lyn-mCherry-FRB were amplified by PCR and inserted into pcDNA3 using the *Eco*RI and *Xho*I sites. Thereafter, DNA fragments encoding TagBFP2 (Evrogen) and TagRFP (a kind gift from Hideki Shibata, Nagoya University) (Shibata *et al.*, 2010) were amplified and inserted in place of mCherry cDNA at the *Age*I and *Bsr*GI sites using an In-Fusion HD cloning kit (Clontech). To construct Lifeact-EGFP and Lifeact-mCherry, sense and antisense oligonucleotides corresponding to the first 17 a.a. of Abp140 (Riedl *et al.*, 2008) were synthesized, annealed, and inserted into pEGFP-N1 (Invitrogen) and pcDNA3-mCherry-N (a kind gift from Roger Tsien, University of California).

### *Cell culture, siRNA-mediated knockdown, and transfection*

HeLa cells were cultured in Minimal Essential Medium (MEM) supplemented with 10% heat-inactivated fetal bovine serum (FBS) at 37°C in 5% $CO_2$. Cells stably expressing HA-tagged P4-ATPases were generated as described previously (Naito *et al.*, 2015, Takatsu *et al.*, 2014). HeLa cells were transfected with plasmids carrying each FKBP-fused fluorescent BAR domain and FRB-fused fluorescent Lyn using X-tremeGENE9 (Roche Applied Science).

siRNAs were prepared as described previously (Naito *et al.*, 2015). In brief, pools of siRNAs targeting the coding region of human ATP10A (nucleotides 655–1399 of ATP10A mRNA; the A nucleotide of the ATG initiation codon was defined as nucleotide 1) were prepared using the T7 RiboMAX Express RNAi System (Promega) and PowerCut Dicer (Fynzymes). Cells were transfected with siRNAs using Lipofectamine 2000 (Invitrogen) and incubated for 24 h. Transfected cells were seeded onto culture dishes. After 24 h, cells were transfected with the siRNAs again and incubated for an additional 24 h. Finally, transfected cells were transferred to new culture dishes containing coverslips, incubated for an additional 48 h, and processed for immunoblot and immunofluorescence analyses.

### *Antibodies and reagents*

Antibodies were obtained from the following sources: monoclonal mouse anti-β-tubulin (KMX-1) (Millipore); monoclonal mouse anti-EEA1 (clone 14), anti-Lamp-1 (H4A3), anti-SNX1 (clone 51), anti-β1-integrin (Mab13), and anti-GM130 (BD Biosciences); monoclonal rat anti-HA (3F10; Roche Applied Science); monoclonal rabbit anti-ATP1A1 (EP1845Y) (Abcam); Alexa Fluor-conjugated secondary antibodies (Molecular Probes); and Cy3- and horseradish peroxidase-conjugated secondary antibodies (Jackson ImmunoResearch

365 Laboratories). Alexa Fluor 488- and 555-conjugated phalloidin was purchased from Molecular

366 Probes. The NBD-labeled phospholipids (Avanti Polar Lipids) used in this study were NBD-

367 PS (1-oleyl-2-[6-[(7-nitro-2-1,3-benzoxadiazol-4-yl)amino]hexanoyl]-sn-glycero-3-

368 phosphoserine), NBD-PE (1-oleyl-2-[6-[(7-nitro-2-1,3-benzoxadiazol-4-yl)amino]hexanoyl]-

369 sn-glycero-3-phosphoethanolamine), and NBD-PC (1-oleyl-2-[6-[(7-nitro-2-1,3-

370 benzoxadiazol-4-yl)amino]hexanoyl]-sn-glycero-3-phosphocholine. Nocodazole, rapamycin,

371 and fibronectin were obtained from Sigma-Aldrich and LC Laboratories, respectively.

372

373 *Immunofluorescence and live-cell imaging*

374 Cells grown on coverslips were treated with 200 nM rapamycin for 15 min, 16.7 μM

375 of nocodazole for 60 min, hypotonic medium (10% MEM and 90% $H_2O$) for 15 min, or

376 hypertonic medium (MEM containing 200 mM sucrose) for 20 min. Time schedule for the

377 treatment(s) was shown in table EV. Treated cells were fixed with 3% paraformaldehyde in

378 PBS at 37°C for 15 min, permeabilized with 0.1% Triton X-100 at room temperature for 5 min,

379 and incubated in PBS containing 10% FBS at room temperature for 30 min. Cells exposed to

380 hypotonic or hypertonic medium were fixed with 3.7% formaldehyde prepared in 0.1× PBS or

381 3.7% formaldehyde prepared in 1× PBS containing 200 mM sucrose, respectively. Fixed cells

382 were incubated with primary antibodies at room temperature for 1 h, washed three times with

383 PBS, and incubated with secondary antibodies at room temperature for 1 h. Coverslips were

384 placed onto Mowiol, and cells were observed using an Axiovert 200M microscope (Carl Zeiss).

385 To obtain semi-quantitative data regarding membrane tubulation, cells containing more than

386 two tubular membrane structures longer than 20 μm, as shown by the epifluorescent signal of

387 each FKBP-BAR domain, were counted. Statistical significance was determined by Welch's t

388 test.

389 For time-lapse recording, cells were placed on a microscope stage prewarmed to

390 37°C, and merged differential interference and fluorescence images were obtained using an

391 A1R-MP confocal laser-scanning microscope (Nikon). Images were acquired every 16.0 sec,

392 and movies play at a rate of 12.5 frames per second.

393

394 *Immunoblotting*

395 Cells were lysed in lysis buffer (20 mM HEPES-KOH [pH 7.4], 150 mM NaCl, 1 mM

396 EDTA, and 1% NP-40) containing a protease inhibitor cocktail (Nacalai Tesque) for 20 min

397 on ice. Cell lysates were centrifuged at 16,100 *g* for 15 min at 4°C in a microcentrifuge. Proteins

12

398 (30 μg) were separated by SDS-PAGE and electroblotted onto an Immobilon-P transfer

399 membrane (Millipore EMD). The membrane was blocked with 5% skimmed milk and

400 sequentially incubated with the indicated primary and horseradish peroxidase-conjugated

401 secondary antibodies. Signals were detected using a Chemi-Lumi One L or Chemi-Lumi One

402 Super kit (Nacalai Tesque).

403

404 ***Flippase assay***

405 Incorporation of NBD-phospholipids was analyzed by flow cytometry as described

406 previously (Takatsu *et al.*, 2014). In brief, HeLa cells were detached from dishes in PBS

407 containing 5 mM EDTA and harvested by centrifugation. Thereafter, cells ($1 \times 10^6$ cells per

408 sample) were washed and equilibrated at 15°C for 15 min in 500 μL Hank's balanced salt

409 solution (pH 7.4) containing 1 g/L glucose (HBSS-glucose). An equal volume of 2 μM NBD-

410 phospholipid prepared in HBSS-glucose was added to the cell suspension and incubated at

411 15°C. At each time point, 200 μL of the cell suspension was collected and mixed with 200 μL

412 of ice-cold HBSS-glucose containing 5% fatty acid-free bovine serum albumin (BSA, Wako

413 Pure Chemical) to extract NBD-lipids incorporated into the exoplasmic leaflet of the PM as

414 well as unincorporated NBD-lipids. Next, 10,000 cells were analyzed on a FACSCalibur

415 instrument (BD Biosciences) to measure the fluorescence of NBD-lipids that had translocated

416 into the cytoplasmic leaflet of the PM. Mean fluorescence intensities per cell were calculated.

417 Propidium iodide-positive cells (i.e., dead cells) were excluded from the analysis.

418 HeLa cells in 12-well plates ($5 \times 10^5$ cells/well) were treated with rapamycin or

419 nocodazole, or were exposed to hypotonic or hypertonic conditions in 500 μL of 0.1× HBSS-

420 glucose or 500 μL HBSS-glucose containing 200 mM sucrose, respectively, at 37°C for the

421 indicated durations. Cells were equilibrated at 15°C for 15 min in the same buffer, and then

422 treated with 500 μL HBSS-glucose containing 2 μM NBD-phospholipid at 15°C for 15 min.

423 Thereafter, cells were detached from the plate and suspended in ice-cold PBS containing 2.5%

424 fatty acid-free BSA, 5 mM EDTA, and 0.04% propidium iodide. Next, 10,000 cells were

425 analyzed on a FACSCalibur instrument. Mean fluorescence intensities per cell were calculated.

426 Propidium iodide-positive cells (i.e., dead cells) were excluded from the analysis.

427

428 ***Uptake of anti-β1-integrin antibody***

429 Cellular uptake of an anti-β1-integrin antibody was assayed using a previously

430 described method with some modifications (Nakai *et al.*, 2013, Shin & Nakayama, 2004,

431     Tanaka *et al.*, 2016). HeLa cells stably expressing ATP10A or ATP10A(E203Q) or *ATP10A*-

432     knockout MDA-MB-231 cells were incubated with an anti-β1-integrin antibody (Mab13) at

433     4°C for 1 h (HeLa cells) or 30 min (MDA-MB-231 cells), washed with ice-cold PBS, and

434     incubated in medium lacking the antibody at 37°C for the indicated durations. Cells were

435     washed with acidic solution (0.5% acetic acid and 0.5 M NaCl, pH 3.0) to remove residual

436     antibodies from the PM prior to fixation. In case of MDA-MB-231 cells, fibronectin-coated

437     cover glass was used to prevent detachment of cells from the cover glass upon temperature

438     shift. Fixed cells were processed for immunofluorescence analysis as described above and

439     imaged using an Axiovert 200 MAT microscope (Carl Zeiss). The fluorescence intensity of

440     intracellular β1-integrin was quantitated using MetaMorph software (Molecular Devices).

441     Variance was assessed by a one-way ANOVA and comparisons were made by Tukey's post-

442     hoc analysis.

443

### RT-PCR

445     Total RNA was isolated from HeLa, MDA-MB-231, RPE-1, and HEK293T cells

446     using an RNeasy mini kit (Qiagen). RT-PCR analysis was performed using a SuperScript III

447     One-Step RT-PCR system (Invitrogen) and the following primer pairs: human CDC50A: sense,

448     GAAAAAGAAAGGTATTGCTTGGTG, antisense, GTAATGTCAGCTGTATTACTACTG;

449     human      ATP10A:      sense,      CACAATGTTCGTGGGCCTCC,      antisense,

450     AAGGACACTGAAGCCACACG; human ATP8B1: sense, GTGGCCTCCACCAACCGGG,

451     antisense,      CACCTCTATTCCTCTGGTTTTCC;      human      ATP8B2:      sense,

452     GGGAGAGAGGCCTGAACCTG, antisense, GGAGTCCAGGATGGCCAGCAG.

453

### Establishment of KO cell lines by the CRISPR/Cas9 system

455     To edit the *ATP10A* gene, we used the CRISPR/Cas9 system described previously

456     (Katoh *et al.*, 2017, Tanaka *et al.*, 2016). Two single guide RNA (sgRNA) sequences (#1 and

457     #2, Figure EV6A) targeting the human *ATP10A* gene were designed using the CRISPR Design

458     Tool from the Zhang lab (http://crispr.mit.edu/). We used a donor plasmid of pDonor-tBFP-

459     NLS-Neo (Addgene #80766) (Tanaka *et al.*, 2016) and PX459 (Addgene #48139). Two

460     plasmids (plasmid containing *ATP10A* target sequences and the Cas9 gene, and a donor

461     plasmid) were introduced into MDA-MB-231 cells by transfection using the X-tremeGENE9

462     DNA Transfection Reagent (Roche). Transfected cells were selected in medium containing

463     G418 (1-4 mg/ml), and clones were isolated on the basis of expression of the reporter gene

464     Tag-BFP. To confirm editing of *ATP10A*, genomic DNA was extracted from individual clones,

465    and subjected to PCR using KOD FX Neo DNA polymerase (TOYOBO). Three primer sets

466    used to amplify *ATP10A* lacking the donor vector integration (S1, 5'-

467    CGAGTGATGATAACCTAAGAGG-3', and AS1, 5'-GTTGATCTTGTGGTCGGAGC-3'),

468    *ATP10A* with donor vector integrated in the forward orientation (donor vector-primer, 5'-

469    GTTGTCCACGGTGCCCTCCATGTAC-3' and S1), and *ATP10A* with donor vector

470    integrated in the reverse orientation (donor vector-primer and AS1). Among clones with donor

471    vector integration in either orientation, the knockout was confirmed by direct sequencing of

472    the amplified PCR product, *ATP10A* without donor vector integration, using a specific

473    sequencing primer (S1 and/or donor vector-primer). Three clones (1-1, 2-1, and 2-6) carrying

474    biallelic changes that resulted in donor vector integration in forward or reverse and frame-

475    shifting indels were used in this study.

476

**Author contributions**

478    HWS, conceived the study and prepared the manuscript. NT, TN, and HT performed

479    experiments. NT, HT, TN, KN, and HWS analyzed the data. All authors discussed the results

480    and commented on the manuscript.

481

**Conflict of interest**

483    The authors declare that they have no conflict of interest.

484

491

**References**

493    Andersen JP, Vestergaard AL, Mikkelsen SA, Mogensen LS, Chalat M, Molday RS (2016) P4-

494    ATPases as Phospholipid Flippases-Structure, Function, and Enigmas. *Front Physiol* 7: 275

495    Bhatia VK, Madsen KL, Bolinger PY, Kunding A, Hedegard P, Gether U, Stamou D (2009)

496    Amphipathic motifs in BAR domains are essential for membrane curvature sensing. *EMBO J*

497    28: 3303-14

498    Campelo F, McMahon HT, Kozlov MM (2008) The hydrophobic insertion mechanism of
499    membrane curvature generation by proteins. *Biophys J* 95: 2325-39

500    Chen CY, Ingram MF, Rosal PH, Graham TR (1999) Role for Drs2p, a P-type ATPase and
501    potential aminophospholipid translocase, in yeast late Golgi function. *J Cell Biol* 147: 1223-36

502    Daleke DL, Huestis WH (1989) Erythrocyte morphology reflects the transbilayer distribution
503    of incorporated phospholipids. *J Cell Biol* 108: 1375-85

504    Devaux PF (1991) Static and dynamic lipid asymmetry in cell membranes. *Biochemistry* 30:
505    1163-1173

506    Devaux PF, Herrmann A, Ohlwein N, Kozlov MM (2008) How lipid flippases can modulate
507    membrane structure. *Biochim Biophys Acta - Biomembr* 1778: 1591-1600

508    Farge E, Ojcius DM, Subtil A, Dautry-Varsat A (1999) Enhancement of endocytosis due to
509    aminophospholipid transport across the plasma membrane of living cells. *Am J Physiol Cell*
510    *Physiol* 276: C725-733

511    Frost A, Perera R, Roux A, Spasov K, Destaing O, Egelman EH, De Camilli P, Unger VM
512    (2008) Structural basis of membrane invagination by F-BAR domains. *Cell* 132: 807-17

513    Frost A, Unger VM, De Camilli P (2009) The BAR domain superfamily: membrane-molding
514    macromolecules. *Cell* 137: 191-6

515    Gallop JL, Jao CC, Kent HM, Butler PJ, Evans PR, Langen R, McMahon HT (2006)
516    Mechanism of endophilin N-BAR domain-mediated membrane curvature. *EMBO J* 25: 2898-
517    910

518    Gauthier NC, Masters TA, Sheetz MP (2012) Mechanical feedback between membrane tension
519    and dynamics. *Trends Cell Biol* 22: 527-35

520    Graham TR (2004) Flippases and vesicle-mediated protein transport. *Trends Cell Biol* 14: 670-
521    7

522    Graham TR, Burd CG (2011) Coordination of Golgi functions by phosphatidylinositol 4-
523    kinases. *Trends Cell Biol* 21: 113-121

524 Hankins HM, Sere YY, Diab NS, Menon AK, Graham TR (2015) Phosphatidylserine
525 translocation at the yeast trans-Golgi network regulates protein sorting into exocytic vesicles.
526 *Mol Biol Cell* 26: 4674-85

527 Henne WM, Kent HM, Ford MG, Hegde BG, Daumke O, Butler PJ, Mittal R, Langen R, Evans
528 PR, McMahon HT (2007) Structure and analysis of FCHo2 F-BAR domain: a dimerizing and
529 membrane recruitment module that effects membrane curvature. *Structure* 15: 839-52

530 Itoh T, De Camilli P (2006) BAR, F-BAR (EFC) and ENTH/ANTH domains in the regulation
531 of membrane-cytosol interfaces and membrane curvature. *Biochim Biophys Acta - Mol Cell*
532 *Biol Lipids* 1761: 897-912

533 Kato U, Inadome H, Yamamoto M, Emoto K, Kobayashi T, Umeda M (2013) Role for
534 Phospholipid Flippase Complex of ATP8A1 and CDC50A Proteins in Cell Migration. *J Biol*
535 *Chem* 288: 4922-4934

536 Katoh Y, Michisaka S, Nozaki S, Funabashi T, Hirano T, Takei R, Nakayama K (2017) Practical
537 method for targeted disruption of cilia-related genes by using CRISPR/Cas9-mediated,
538 homology-independent knock-in system. *Mol Biol Cell* 28: 898-906

539 Komatsu T, Kukelyansky I, McCaffery JM, Ueno T, Varela LC, Inoue T (2010) Organelle-
540 specific, rapid induction of molecular activities and membrane tethering. *Nat Meth* 7: 206-208

541 Lee S, Uchida Y, Wang J, Matsudaira T, Nakagawa T, Kishimoto T, Mukai K, Inaba T,
542 Kobayashi T, Molday RS, Taguchi T, Arai H (2015) Transport through recycling endosomes
543 requires EHD1 recruitment by a phosphatidylserine translocase. *EMBO J* 34: 669-88

544 Masters TA, Pontes B, Viasnoff V, Li Y, Gauthier NC (2013) Plasma membrane tension
545 orchestrates membrane trafficking, cytoskeletal remodeling, and biochemical signaling during
546 phagocytosis. *Proc Natl Acad Sci U S A* 110: 11875-11880

547 Masuda M, Takeda S, Sone M, Ohki T, Mori H, Kamioka Y, Mochizuki N (2006) Endophilin
548 BAR domain drives membrane curvature by two newly identified structure-based mechanisms.
549 *EMBO J* 25: 2889-97

550 McMahon HT, Boucrot E (2015) Membrane curvature at a glance. *J Cell Sci* 128: 1065-1070

551    Miyano R, Matsumoto T, Takatsu H, Nakayama K, Shin HW (2016) Alteration of transbilayer
552    phospholipid compositions is involved in cell adhesion, cell spreading, and focal adhesion
553    formation. *FEBS Lett* 590: 2138-45

554    Murate M, Abe M, Kasahara K, Iwabuchi K, Umeda M, Kobayashi T (2015) Transbilayer
555    distribution of lipids at nano scale. *J Cell Sci* 128: 1627-38

556    Muthusamy B-P, Natarajan P, Zhou X, Graham TR (2009) Linking phospholipid flippases to
557    vesicle-mediated protein transport. *Biochim Biophys Acta - Mol Cell Biol Lipids*, pp 612-619.

558    Naito T, Takatsu H, Miyano R, Takada N, Nakayama K, Shin HW (2015) Phospholipid Flippase
559    ATP10A Translocates Phosphatidylcholine and Is Involved in Plasma Membrane Dynamics. *J*
560    *Biol Chem* 290: 15004-17

561    Nakai W, Kondo Y, Saitoh A, Naito T, Nakayama K, Shin H-W (2013) ARF1 and ARF4
562    regulate recycling endosomal morphology and retrograde transport from endosomes to the
563    Golgi apparatus. *Mol Biol Cell* 24: 2570-2581

564    Op den Kamp JA (1979) Lipid asymmetry in membranes. *Annu Rev Biochem* 48: 47-71

565    Panatala R, Hennrich H, Holthuis JC (2015) Inner workings and biological impact of
566    phospholipid flippases. *J Cell Sci* 128: 2021-32

567    Peter BJ, Kent HM, Mills IG, Vallis Y, Butler PJG, Evans PR, McMahon HT (2004) BAR
568    Domains as Sensors of Membrane Curvature: The Amphiphysin BAR Structure. *Science* 303:
569    495-499

570    Poudel KR, Dong Y, Yu H, Su A, Ho T, Liu Y, Schulten K, Bai J (2016) A time course of
571    orchestrated endophilin action in sensing, bending, and stabilizing curved membranes. *Mol*
572    *Biol Cell* 27: 2119-32

573    Riedl J, Crevenna AH, Kessenbrock K, Yu JH, Neukirchen D, Bista M, Bradke F, Jenne D,
574    Holak TA, Werb Z, Sixt M, Wedlich-Soldner R (2008) Lifeact: a versatile marker to visualize
575    F-actin. *Nat Meth* 5: 605-7

576    Segawa K, Kurata S, Nagata S (2016) Human Type IV P-type ATPases That Work as Plasma
577    Membrane Phospholipid Flippases and Their Regulation by Caspase and Calcium. *J Biol Chem*

578   291: 762-72

579   Seigneuret M, Devaux PF (1984) ATP-dependent asymmetric distribution of spin-labeled

580   phospholipids in the erythrocyte membrane: relation to shape changes. *Proc Natl Acad Sci U S*

581   *A* 81: 3751-5

582   Sheetz MP, Singer SJ (1974) Biological membranes as bilayer couples. A molecular mechanism

583   of drug-erythrocyte interactions. *Proc Natl Acad Sci U S A* 71: 4457-61

584   Shi Z, Baumgart T (2015) Membrane tension and peripheral protein density mediate membrane

585   shape transitions. *Nat Commun* 6: 5974

586   Shibata Y, Shemesh T, Prinz WA, Palazzo AF, Kozlov MM, Rapoport TA (2010) Mechanisms

587   Determining the Morphology of the Peripheral ER. *Cell* 143: 774-788

588   Shin H-W, Nakayama K (2004) Guanine Nucleotide-Exchange Factors for Arf GTPases: Their

589   Diverse Functions in Membrane Traffic. *J Biochem (Tokyo)* 136: 761-767

590   Suarez A, Ueno T, Huebner R, McCaffery JM, Inoue T (2014) Bin/Amphiphysin/Rvs (BAR)

591   family members bend membranes in cells. *Sci Rep* 4: 4693

592   Takatsu H, Baba K, Shima T, Umino H, Kato U, Umeda M, Nakayama K, Shin H-W (2011)

593   ATP9B, a P4-ATPase (a Putative Aminophospholipid Translocase), Localizes to the trans-

594   Golgi Network in a CDC50 Protein-independent Manner. *J Biol Chem* 286: 38159-38167

595   Takatsu H, Takayama M, Naito T, Takada N, Tsumagari K, Ishihama Y, Nakayama K, Shin HW

596   (2017) Phospholipid flippase ATP11C is endocytosed and downregulated following Ca2+-

597   mediated protein kinase C activation. *Nat Commun* 8: 1423

598   Takatsu H, Tanaka G, Segawa K, Suzuki J, Nagata S, Nakayama K, Shin HW (2014)

599   Phospholipid Flippase Activities and Substrate Specificities of Human Type IV P-type ATPases

600   Localized to the Plasma Membrane. *J Biol Chem* 289: 33543-33556

601   Takeda M, Yamagami K, Tanaka K (2014) Role of phosphatidylserine in phospholipid flippase-

602   mediated vesicle transport in Saccharomyces cerevisiae. *Eukaryot Cell* 13: 363-75

603   Tanaka Y, Ono N, Shima T, Tanaka G, Katoh Y, Nakayama K, Takatsu H, Shin HW (2016) The

604    phospholipid flippase ATP9A is required for recycling pathway from endosomes to the plasma

605    membrane. *Mol Biol Cell* 27: 3883-93

606    Xu P, Baldridge RD, Chi RJ, Burd CG, Graham TR (2013) Phosphatidylserine flipping

607    enhances membrane curvature and negative charge required for vesicular transport. *J Cell Biol*

608    202: 875-86

609    Yabas M, Coupland LA, Cromer D, Winterberg M, Teoh NC, D'Rozario J, Kirk K, Broer S,

610    Parish CR, Enders A (2014) Mice Deficient in the Putative Phospholipid Flippase ATP11C

611    Exhibit Altered Erythrocyte Shape, Anemia and Reduced Erythrocyte Lifespan. *J Biol Chem*

612    289: 19531-19537

613    Yin Y, Arkhipov A, Schulten K (2009) Simulations of membrane tubulation by lattices of

614    amphiphysin N-BAR domains. *Structure* 17: 882-92

615    Zachowski A (1993) Phospholipids in animal eukaryotic membranes: transverse asymmetry

616    and movement. *Biochem J* 294 ( Pt 1): 1-14

617    Zhu X, Libby RT, de Vries WN, Smith RS, Wright DL, Bronson RT, Seburn KL, John SW

618    (2012) Mutations in a P-type ATPase gene cause axonal degeneration. *PLoS Genet* 8: e1002853

619

620 **Figure legends**

621

622 **Figure 1. Enhancement of PC-flippase activity at the PM upon expression of ATP10A**

623 **triggers membrane tubulation by PM-recruited ΔN-BAR and F-BAR domains**

624 HeLa cells stably expressing C-terminally HA-tagged ATP10A, ATP10A(E203Q), and

625 ATP11A were transiently co-transfected with expression vectors for Lyn-TagBFP2-FRB (PM)

626 and EGFP-FKBP-N-BAR (N-BAR), EGFP-FKBP-ΔN-BAR (ΔN-BAR), or mCherry-FKBP-

627 F-BAR (F-BAR). Cells were treated with vehicle alone [Rapa(−)] or 200 nM rapamycin [Rapa

628 (+)] for 15 min and fixed. Fixed cells were stained for an anti-HA primary antibody, followed

629 by a Cy3-conjugated (A–C, G–I) or Alexa Fluor 488-conjugated (D–F) anti-rat secondary

630 antibody. Panels b' and d' show enlarged images of the insets in b and d, respectively. Bars,

631 20 μm. Bars in enlarged images, 2 μm. (J–L) Cells containing membrane tubules were counted

632 [420–672 cells (ΔN-BAR), 417–527 cells (F-BAR), and 422–805 cells (N-BAR) per sample].

633 Graphs display means ± SD of three independent experiments. **, $p < 0.01$; ***, $p < 0.005$.

634

635 **Figure 2. Expression of ATP10A does not affect the integrity of the actin cytoskeleton or**

636 **microtubules**

637 HeLa cells stably expressing C-terminally HA-tagged ATP10A or ATP10A(E203Q) were

638 transiently co-transfected with expression vectors for Lyn-TagBFP2-FRB (PM) and EGFP-

639 FKBP-ΔN-BAR (ΔN-BAR). Cells were treated with 200 nM rapamycin for 15 min and fixed.

640 Fixed cells were permeabilized and incubated with Alexa Fluor 555-conjugated phalloidin (A),

641 or stained with an anti-β-tubulin primary antibody followed by an Alexa Fluor 555-conjugated

642 anti-mouse secondary antibody (B). Panels a', and d'–i' show enlarged images of the insets in

643 a, and d–i, respectively. Bars, 20 μm. Bars in enlarged images, 2 μm.

644

645 **Figure 3. Disruption of microtubules reduced tubular structures caused by PM-recruited**

646 **BAR-domains**

647 (A, B, E) HeLa cells were transiently co-transfected with expression vectors for Lyn-TagBFP2-

648 FRB (PM) and EGFP-FKBP-N-BAR (N-BAR), or EGFP-FKBP-ΔN-BAR (ΔN-BAR). (C, D,

649 F, G) HeLa cells stably expressing HA-tagged ATP10A were transiently co-transfected with

650 expression vectors for Lyn-TagBFP2-FRB (PM) and EGFP-FKBP-ΔN-BAR (ΔN-BAR), or

651 mCherry-FKBP-F-BAR (F-BAR). (A–G) Transfected cells were pretreated with vehicle alone

652 (Mock) or Nocodazole (Noz). The cells were further treated with vehicle alone or nocodazole

21

in the presence of rapamycin. Cells were fixed, permeabilized and stained with antibody against β-tubulin followed by Alexa Fluor 555– or Alexa Fluor 488–conjugated anti-mouse secondary antibody. Panels of b', c', e', e'', f', and f'' are enlarged images of insets in b, c, e, and f. Bars, 20 μm. Bars in enlarged images, 2 μm. (E–G) Cells containing membrane tubules were counted [429–492 cells (E), 397–479 cells (F), and 404-436 cells (G) in each sample]. Graphs display means ± SD from three independent experiments. *, $p < 0.05$; ****, $p < 0.001$. The experiments of (G) were performed together with Fig. 5F and thus the graph of Mock is equivalent to that of Fig. 5F.

**Figure 4. Hypotonic treatment of HeLa cells prevents membrane tubulation induced by the PM-recruited N-BAR domain**

HeLa cells were transiently co-transfected with expression vectors for Lyn-TagBFP2-FRB (PM) and EGFP-FKBP-N-BAR (N-BAR) or EGFP-FKBP-ΔN-BAR (ΔN-BAR). (A–D) Transfected cells were incubated in isotonic medium containing rapamycin (Mock) or exposed to hypotonic or hypertonic medium containing rapamycin. Cells were fixed, permeabilized, and incubated with Alexa Fluor 555-conjugated phalloidin. Panels b', c', e', and f' show enlarged images of the insets in b, c, e, and f, respectively. Bars, 20 μm. Bars in enlarged images, 2 μm. (E, F, G) Cells containing membrane tubules were counted [416–577 cells (N-BAR) and 402–467 cells (ΔN-BAR) per sample]. Graphs display means ± SD of three independent experiments. ***, $p < 0.005$.

**Figure 5. Hypotonic treatment of ATP10A-expressing cells prevents membrane tubulation induced by PM-recruited ΔN-BAR and F-BAR domains**

HeLa cells stably expressing C-terminally HA-tagged ATP10A were transiently co-transfected with expression vectors for Lyn-TagBFP2-FRB (PM) and EGFP-FKBP-ΔN-BAR (ΔN-BAR) (A, B, E) or mCherry-FKBP-F-BAR (F-BAR) (C, D, F). Transfected cells were incubated in isotonic medium containing rapamycin (Mock) or exposed to hypotonic or hypertonic medium containing rapamycin. Cells were fixed, permeabilized, and incubated with Alexa Fluor 555-conjugated (A, B) or Alexa Fluor 488-conjugated (C, D) phalloidin. Panels b', c', e', and f' show enlarged images of the insets in b, c, e, and f, respectively. Bars, 20 μm. Bars in enlarged images, 2 μm. (E, F) Cells containing membrane tubules were counted [400–452 cells (ΔN-BAR) and 404–436 cells (F-BAR) per sample]. Graphs display means ± SD of three independent experiments. **, $p < 0.01$; ***, $p < 0.005$.

686

**Figure 6. Depletion of ATP10A abrogates membrane tubulation induced by ΔN-BAR and**

**F-BAR domains in ATP10A-expressing cells**

HeLa cells stably expressing HA-tagged ATP10A were transfected with a pool of siRNAs

against LacZ (as a control) or ATP10A. After 96 h, cells were transiently co-transfected with

expression vectors for Lyn-TagBFP2-FRB (PM) and EGFP-FKBP-N-BAR (N-BAR), EGFP-

FKBP-ΔN-BAR (ΔN-BAR), or mCherry-FKBP-F-BAR (F-BAR). Cells were treated with

vehicle alone [Rapa(−)] or 200 nM rapamycin [Rapa(+)] for 15 min and fixed. Fixed cells were

stained with an anti-HA primary antibody followed by a Cy3-conjugated (A, E) or Alexa Fluor

488-conjugated (C) anti-rat secondary antibody. Bars, 20 μm. Bars in enlarged images, 2 μm.

(B, D, F) Cells containing membrane tubules were counted [410–535 cells (ΔN-BAR), 389–

464 cells (F-BAR), and 331–645 cells (N-BAR) per sample]. Graphs display means ± SD of

three independent experiments. **, $p < 0.01$; ***, $p < 0.005$.

699

**Figure 7. Expression of ATP10A increases the internalization rate of β1-integrin**

HeLa cells stably expressing C-terminally HA-tagged ATP10A, ATP10A(E203Q), or

ATP11A were incubated with an anti-β1-integrin antibody at 4°C for 1 h, washed with ice-cold

PBS to remove unbound antibodies, and incubated at 37°C for the indicated durations to allow

internalization of β1-integrin. Cells were washed with acidic solution to remove residual

antibodies on the PM prior to fixation. Fixed cells were permeabilized and incubated with a

Cy3-conjugated anti-rat secondary antibody and Alexa Fluor 488-conjugated phalloidin. (A)

Representative images are displayed. Insets show phalloidin staining. Bars, 20 μm. (B)

Fluorescence intensities of internalized β1-integrin were quantitated using MetaMorph

software. A total of 115–224 cells were analyzed per sample. Graphs display means ± SD of

four independent experiments. *, $p < 0.05$; **, $p < 0.01$; ***, $p < 0.005$.

711

**Figure 8. Schematic illustration of the sensing and/or generation of membrane curvature**

**by BAR domains**

(A) Penetration of the N-terminal amphipathic helix of the N-BAR domain has a wedging

effect, leading to increased membrane curvature into the cytoplasm. The N-BAR domain

subsequently senses this membrane curvature and triggers membrane tubulation by

oligomerizing along the membrane (PDB: 4ATM, N-BAR domain of amphiphysin 1). (B) By

contrast, the ΔN-BAR domain, which lacks the amphipathic helix, cannot generate membrane

23

719 curvature by itself, but can still sense membrane curvature. Thus, the ΔN-BAR domain can

720 generate membrane tubulation following induction of membrane deformation by P4-ATPases.

721 **EV Figure Legends**

722 **Figure EV1. Membrane tubulation is induced by recruitment of the N-BAR domain, but**

723 **not of the ΔN-BAR or F-BAR domain, to the PM**

724 (A) Schematic illustration of the CID system that allows acute recruitment of BAR domains to

725 the PM following treatment with rapamycin. FP, fluorescent protein; FKBP, FK506-binding

726 protein; FRB, FKBP-rapamycin-binding domain. (B–D) HeLa cells were transiently co-

727 transfected with expression vectors for Lyn-TagBFP2-FRB (PM) and EGFP-FKBP-N-BAR

728 (N-BAR), EGFP-FKBP-ΔN-BAR (ΔN-BAR), or mCherry-FKBP-F-BAR (F-BAR). After 24

729 h, cells were treated with vehicle alone [Rapa(−)] or 200 nM rapamycin [Rapa(+)] for 15 min,

730 fixed, and observed using an epifluorescence microscope. Panels b', b", d', and d" show

731 enlarged images of the insets in b and d. (E) HeLa cells were transiently co-transfected with

732 expression vectors for Lyn-TagBFP2-FRB (PM) and EGFP-FKBP-N-BAR (N-BAR). After 24

733 h, cells were treated with 200 nM rapamycin for 15 min, fixed, and stained with an antibody

734 against EEA1, Lamp-1, sorting nexin 1 (SNX1), or GM130 (markers of early endosomes, late

735 endosomes/lysosomes, endosomes, and the Golgi complex, respectively) followed by an Alexa

736 Fluor 555-conjugated anti-mouse secondary antibody.

737

738 **Figure EV2. Flippase activity in ATP10A-expressing cells**

739 (A) HeLa cells stably expressing HA-tagged P4-ATPases were lysed and subjected to SDS-

740 PAGE and immunoblotting with an anti-HA or anti-β-tubulin antibody to determine the total

741 level of the P4-ATPase protein. (B) HeLa cells stably expressing P4-ATPases were treated

742 with vehicle alone [Rapa(−)] or 200 nM rapamycin [Rapa(+)] for 15 min. (C) HeLa cells stably

743 expressing ATP10A were mock-transfected (Mock) or transiently co-transfected with

744 expression vectors for Lyn-TagRFP-FRB (PM) and mCherry-FKBP, mCherry-FKBP-ΔN-

745 BAR (ΔN-BAR), or mCherry-FKBP-N-BAR (N-BAR). After 24 h, cells were treated with 200

746 nM rapamycin. (D, E) HeLa cells stably expressing P4-ATPases were treated with vehicle

747 alone (Mock), or 16.7 μM of nocodazole or incubated in isotonic, hypotonic, or hypertonic

748 medium. (B–E) Cells were then incubated with the indicated NBD-lipids at 15°C for 15 min.

749 After extraction with fatty acid-free BSA, the residual fluorescence intensity associated with

750 cells was determined by flow cytometry. The fold increase in NBD-lipid uptake relative to that

751 in vector-infected control cells (−) (B and D) or mCherry-FKBP-transfected cells (FKBP, (−))

752 (C) is shown. Graphs display means ± SD of three independent experiments.

753

754 **Figure EV3. PM-recruited ΔN-BAR and F-BAR domains do not induce membrane**

755 **tubulation in ATP10A(E203Q)-expressing cells**

756 HeLa cells stably expressing C-terminally HA-tagged ATP10A(E203Q) were transiently co-

757 transfected with expression vectors for Lyn-TagBFP2-FRB (PM) and EGFP-FKBP-ΔN-BAR

758 (ΔN-BAR) (A, B) or mCherry-FKBP-F-BAR (F-BAR) (C, D). Transfected cells were

759 incubated in isotonic medium containing rapamycin (Mock) or exposed to hypotonic or

760 hypertonic medium containing rapamycin. Cells were fixed, permeabilized, and incubated with

761 Alexa Fluor 555- or 488-conjugated phalloidin. Bars, 20 μm. Bars in enlarged images, 2 μm.

762

763 **Figure EV4. Depletion of ATP10A in ATP10A-expressing cells**

764 (A) RT-PCR was performed using total RNA isolated from the indicated cell lines. RNA was

765 omitted in control reactions. (B) HeLa cells stably expressing HA-tagged ATP10A were treated

766 with a pool of siRNAs targeting LacZ or ATP10A. After 120 h, cells were lysed and subjected

767 to SDS-PAGE and immunoblotting with an anti-HA or anti-β-tubulin antibody. (−) indicates

768 parental HeLa cells. (C) Cells treated with a pool of siRNAs targeting LacZ or ATP10A were

769 incubated with NBD-PC at 15°C as described in the legend of Figure EV2. The fold increase

770 in NBD-PC uptake relative to that in parental cells is shown. Graphs display means ± SD of

771 three independent experiments.

772

773 **Figure EV5. ATP1A1 localization in ATP10A-expressing cells**

774 HeLa cells stably expressing C-terminally HA-tagged ATP10A, and ATP10A(E203Q) were

775 fixed and stained for an anti-HA and anti-ATP1A1 primary antibodies, followed by a Cy3-

776 conjugated anti-rat and Alexa488-conjugated anti-rabbit secondary antibodies. (A) Bars, 20

777 μm. (B) Cells in which ATP1A1 localized to the plasma membrane (black), or to the plasma

778 membrane and intracellular puncta (white) were counted: counts were normalized against the

779 total number of counted cells (562-644 cells). Graphs display means of two independent

780 experiments and error bars show minimum and maximum values.

781

782 **Figure EV6. Internalization of β1-integrin in *ATP10A*-knockout (KO) cells**

783     *ATP10A* gene of MDA-MB-231 cells was edited by the CRISPR/Cas9 system. (A) Target

784     sequences of *ATP10A* gene are shown. (B) In clone 1-1, clone 2-1, and clone 2-6, *ATP10A*

785     carries biallelic modifications: insertion of a base and donor vector (reverse integration),

786     deletion of 31 bases and insertion of donor vector (forward integration), and deletion of a base

787     and insertion of donor vector (forward integration), respectively. (C) Parental MDA-MB-231

788     cells (-) and *ATP10A*-KO cell lines were incubated with an anti-β1-integrin antibody at 4°C for

789     30 min, washed with ice-cold PBS to remove unbound antibodies, and incubated at 37°C for

790     30 min to allow internalization of β1-integrin. Cells were washed with acidic solution to

791     remove residual antibodies on the PM prior to fixation. Fixed cells were permeabilized and

792     incubated with a Cy3-conjugated anti-rat secondary antibody. Fluorescence intensities of

793     internalized β1-integrin were quantitated using MetaMorph software. A total of 70–174 cells

794     were analyzed per sample. Graphs display means ± SD of three independent experiments. (D)

795     RT-PCR was performed using total RNA isolated from the indicated cell lines. RNA was

796     omitted in control reactions.

797

798     **EV Table Legend**

799     **Table EV. Time schedule for treatment(s) of cells**

800     Arrows indicate the treatments of cells. Rapa, rapamycin; Noz, nocodazole; Hypo, hypotonic

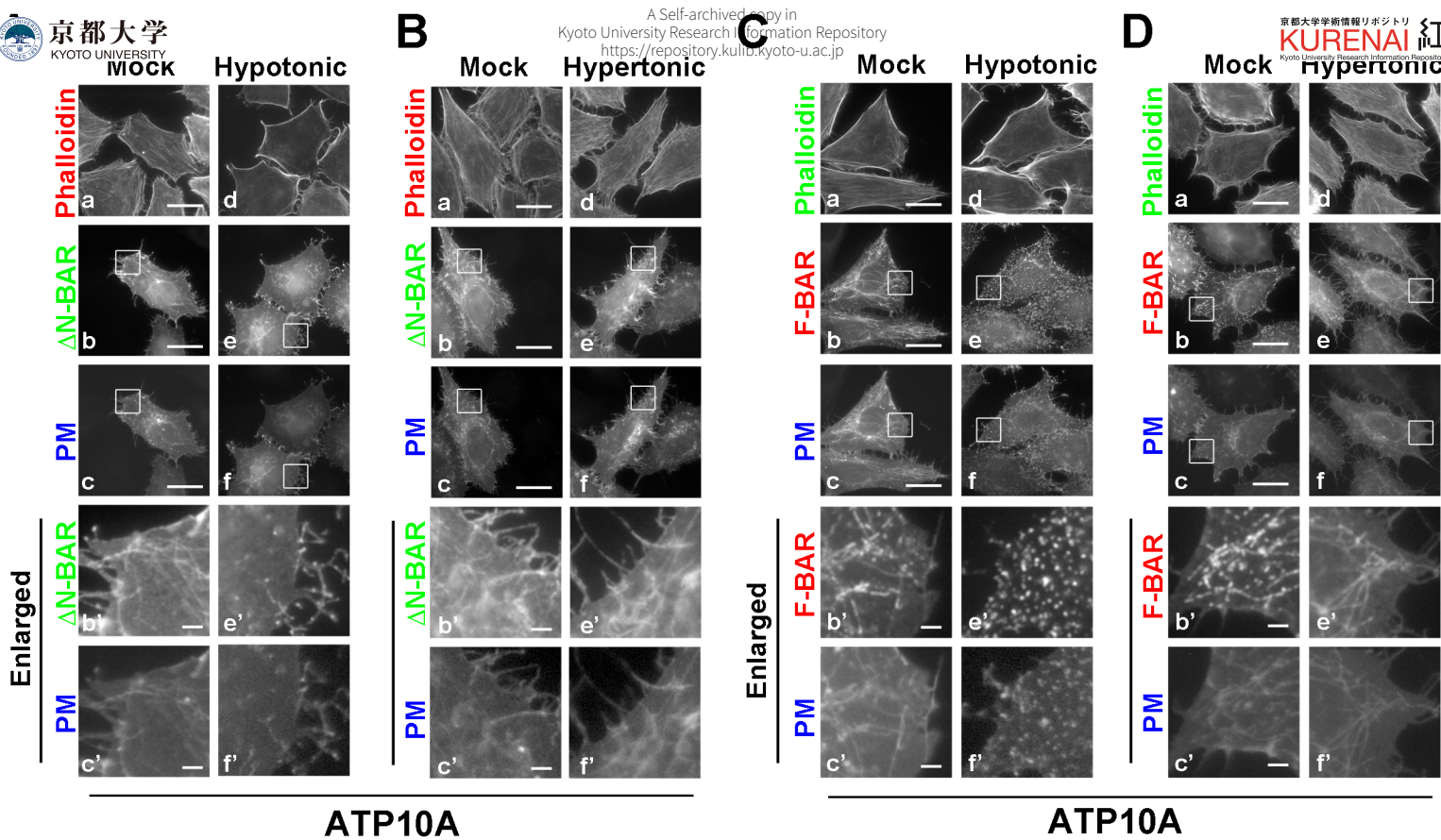801     stress; Hyper, hypertonic stress

802
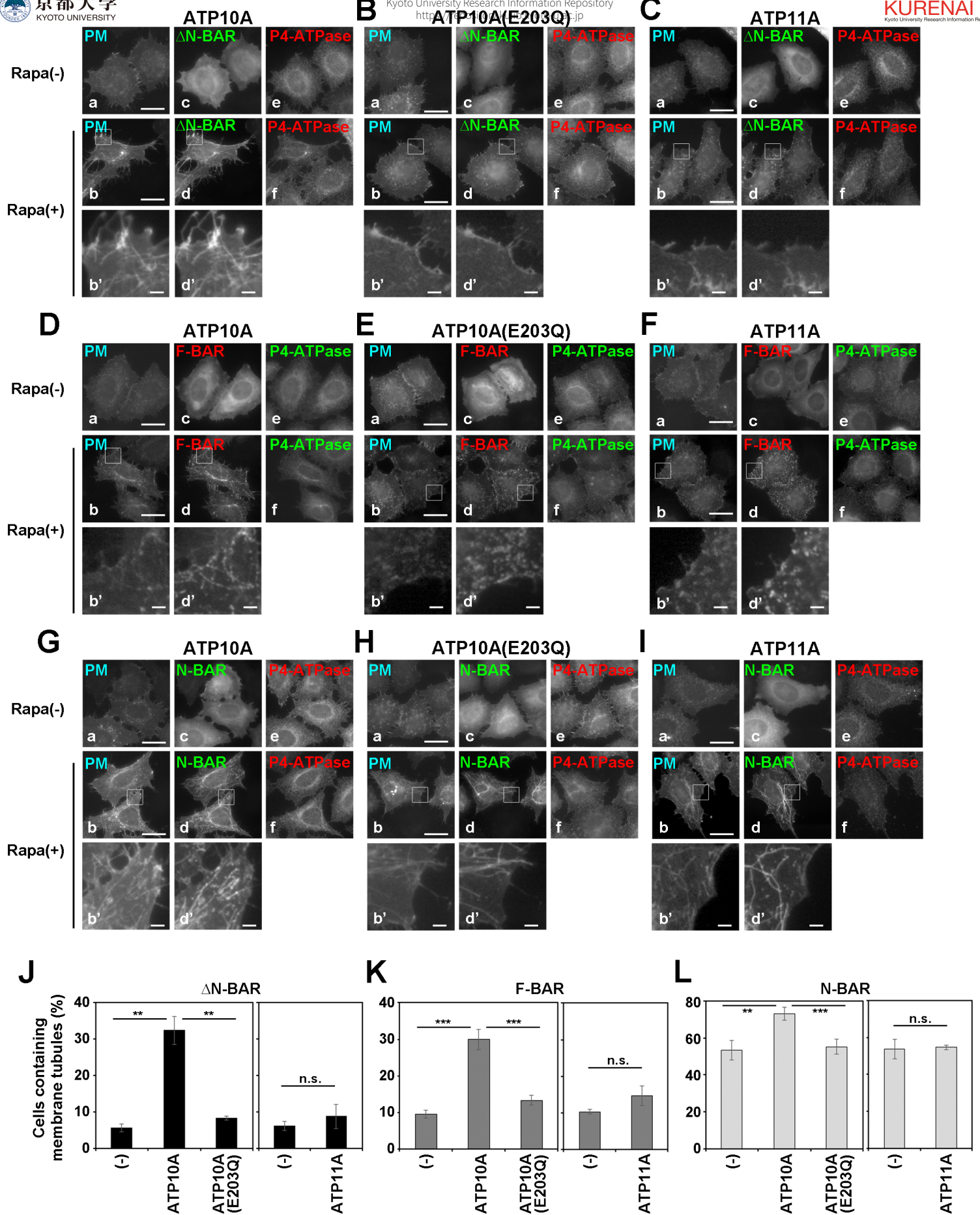
Figure 1. Takada et al.
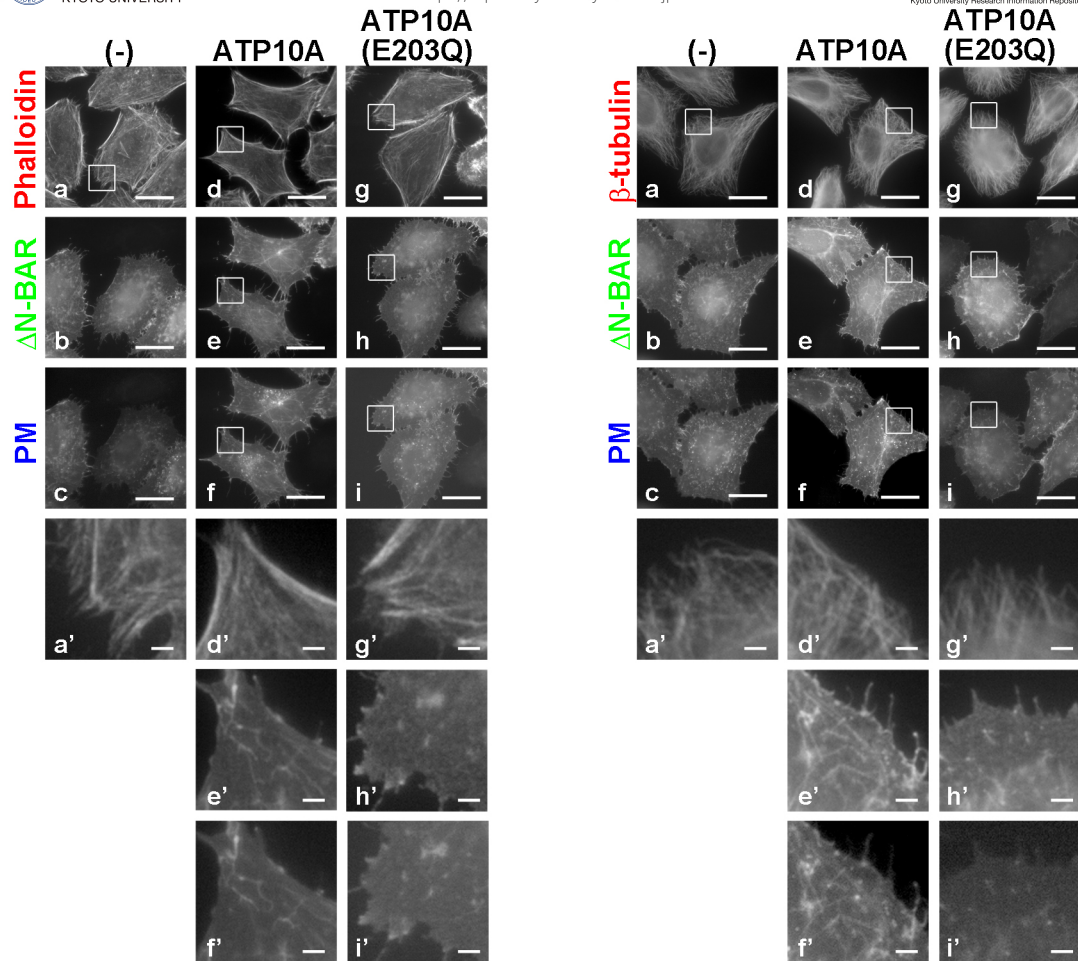
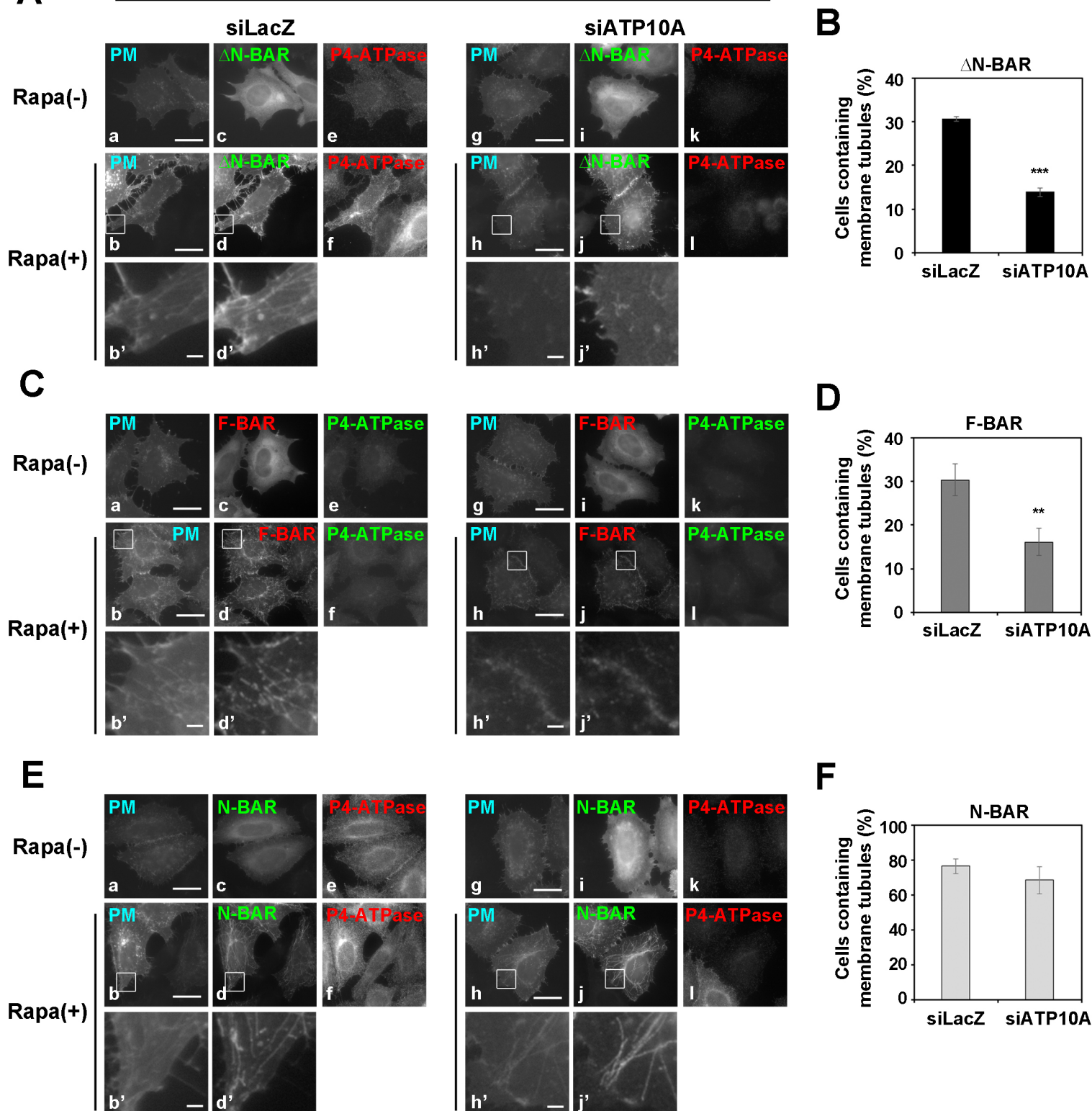**Figure 2 Takada et al.**
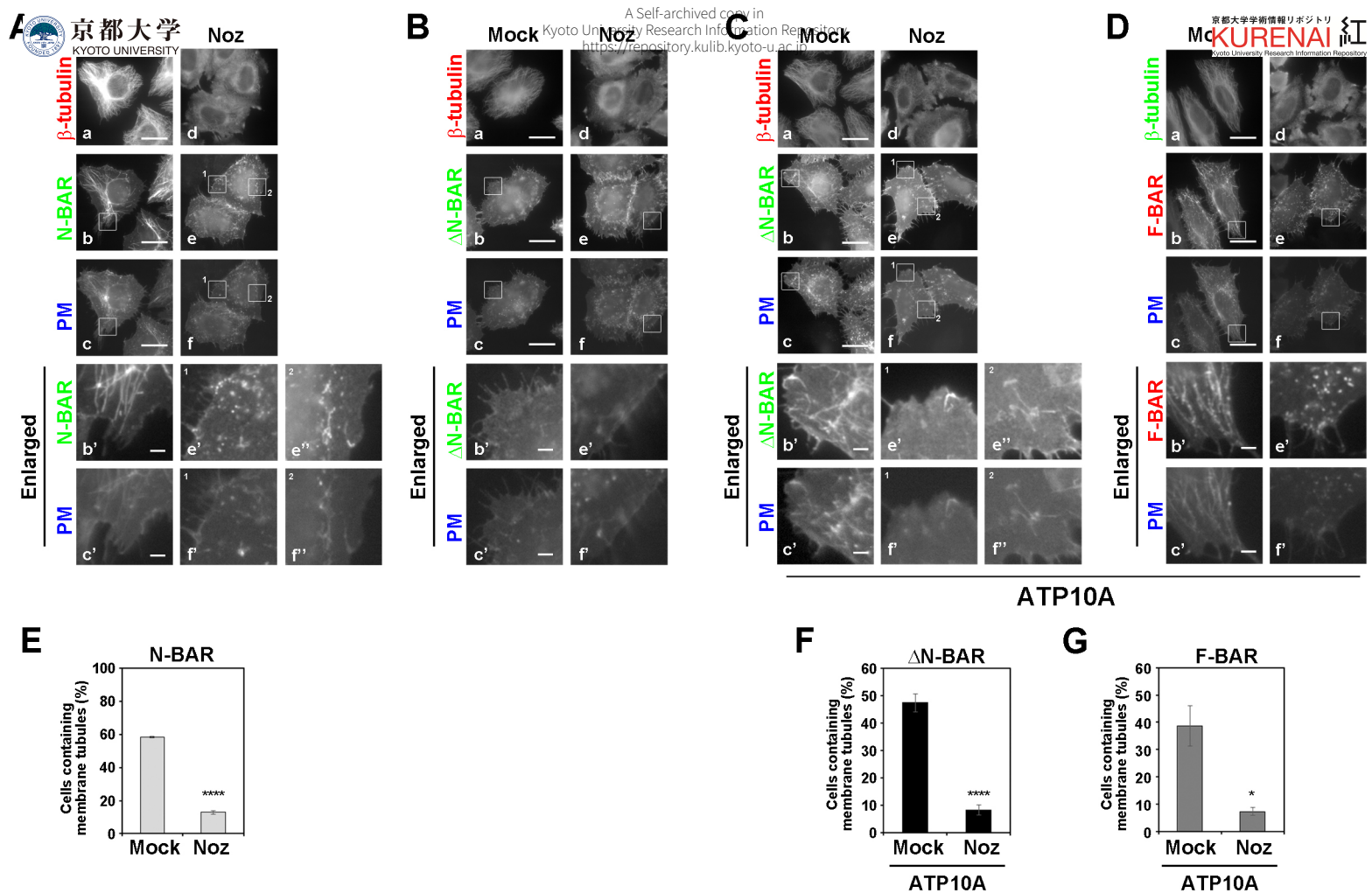
Figure 3 Takada et al.
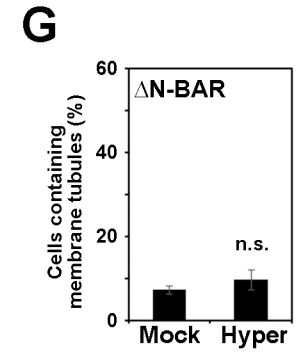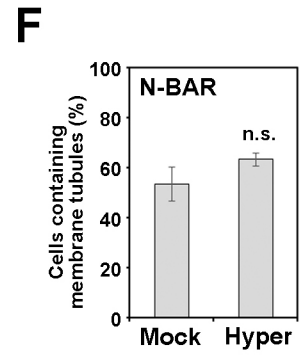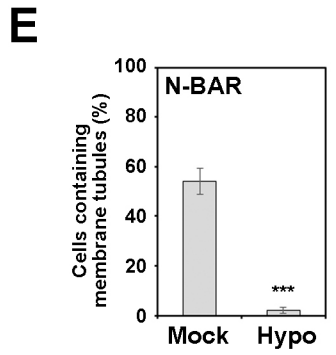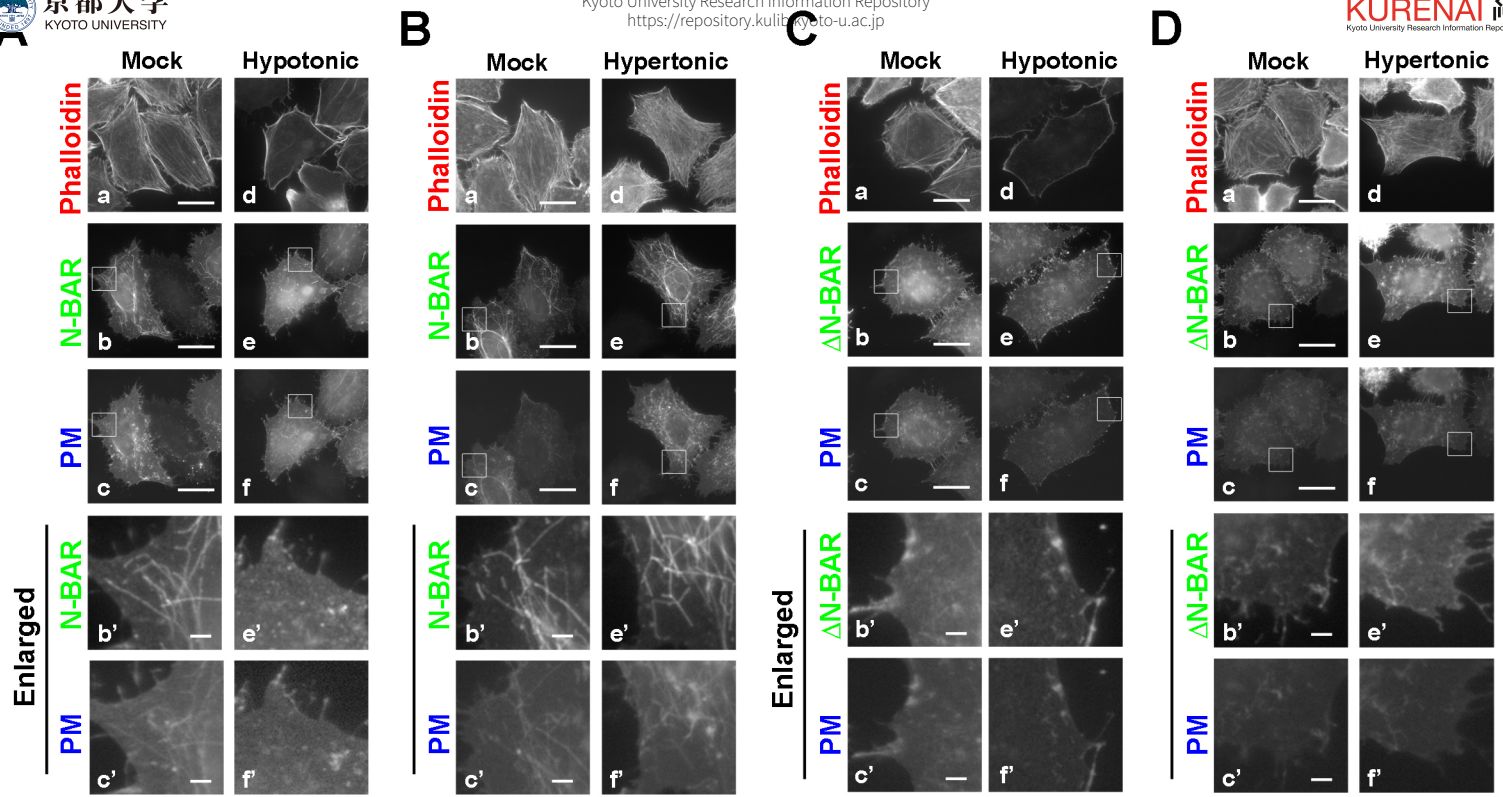
Figure 4 Takada et al.

**Figure 5 Takada et al.**
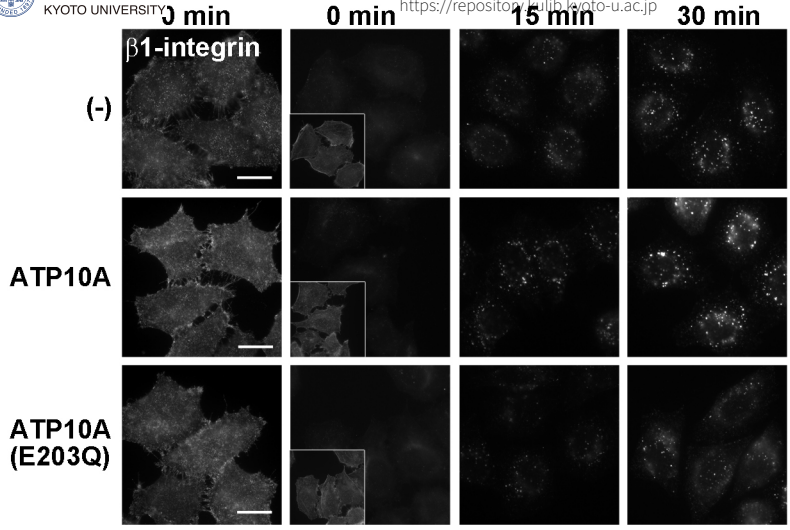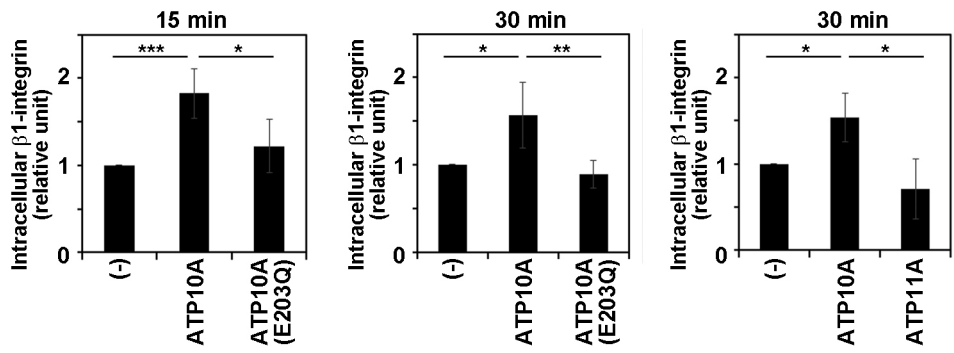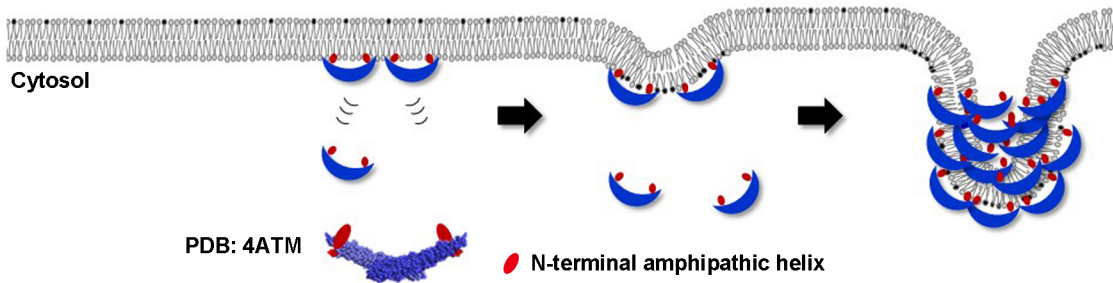
**ATP10A-HA-expressing cells**
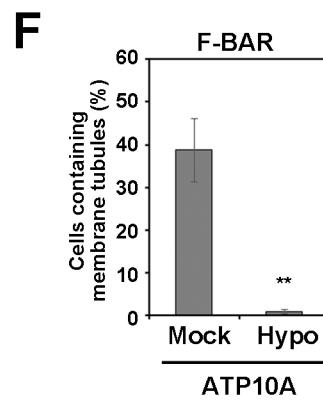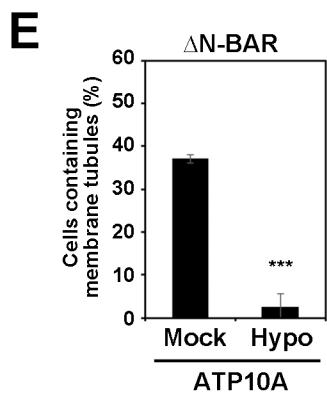


**Figure 6 Takada et al.**

Figure 7. Takada et al.

**N-BAR**
**Curvature generating and sensing**

PDB: 4ATM

🔴 N-terminal amphipathic helix
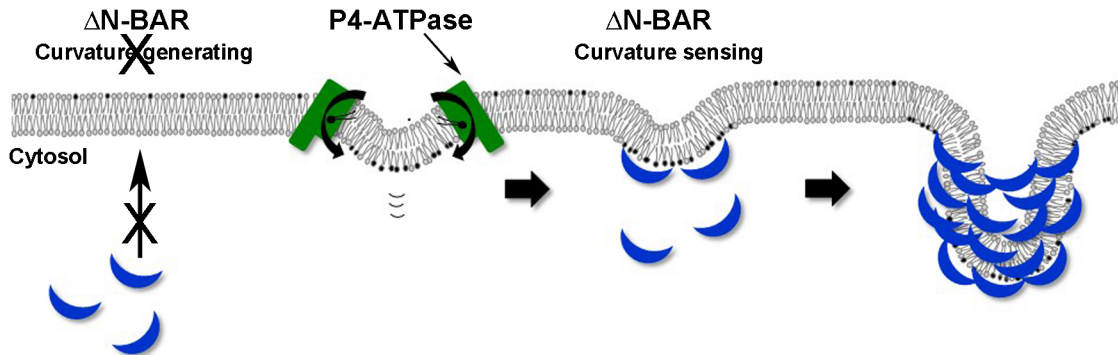
**B**

ΔN-BAR
Curvature generating

P4-ATPase
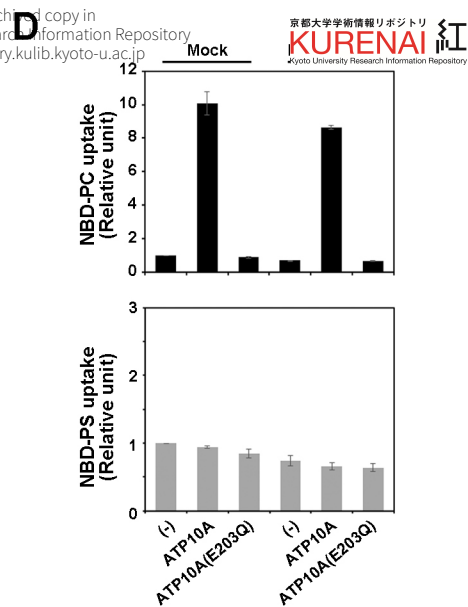
ΔN-BAR
Curvature sensing

Cytosol

**Figure 8 Takada et al.**
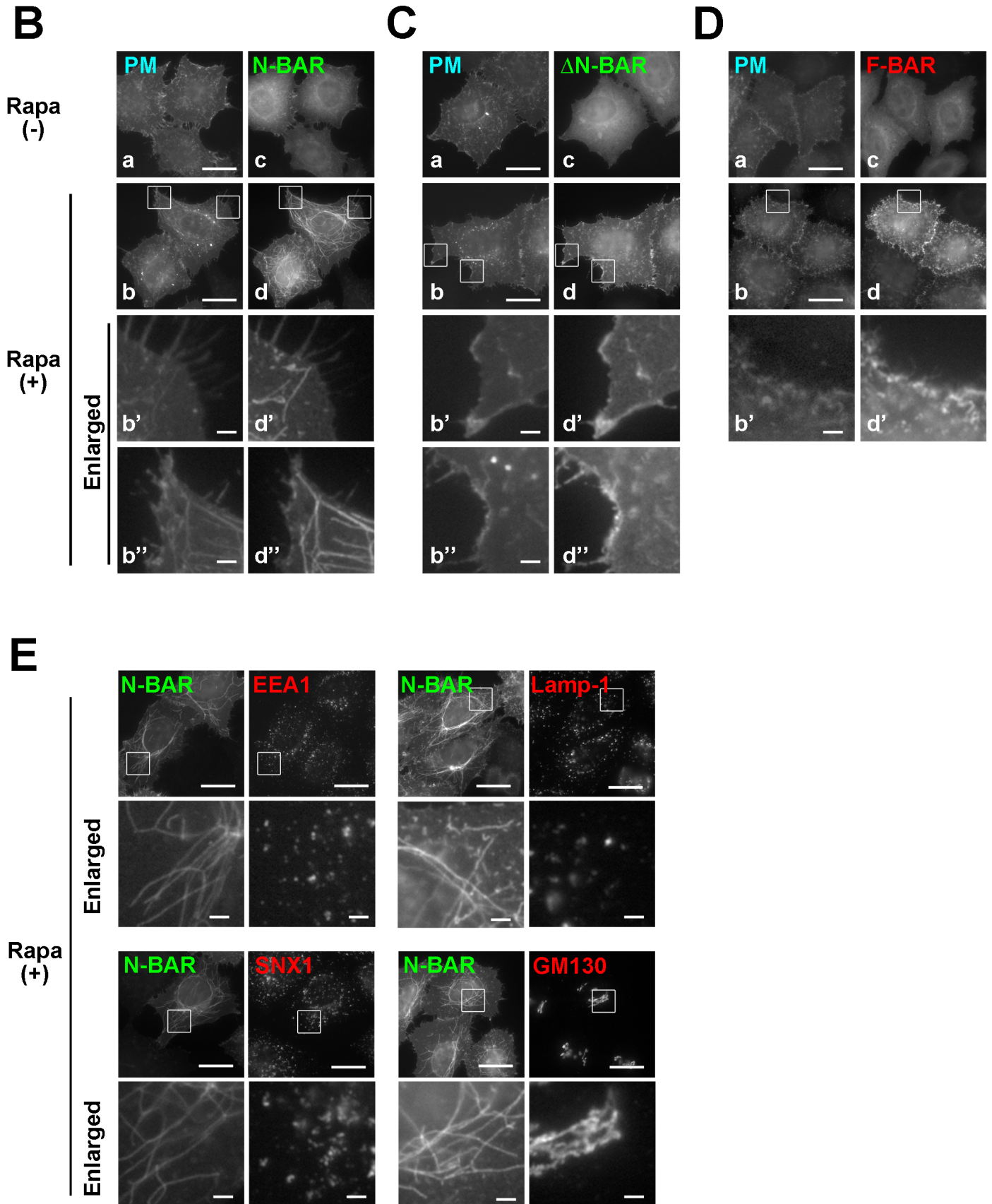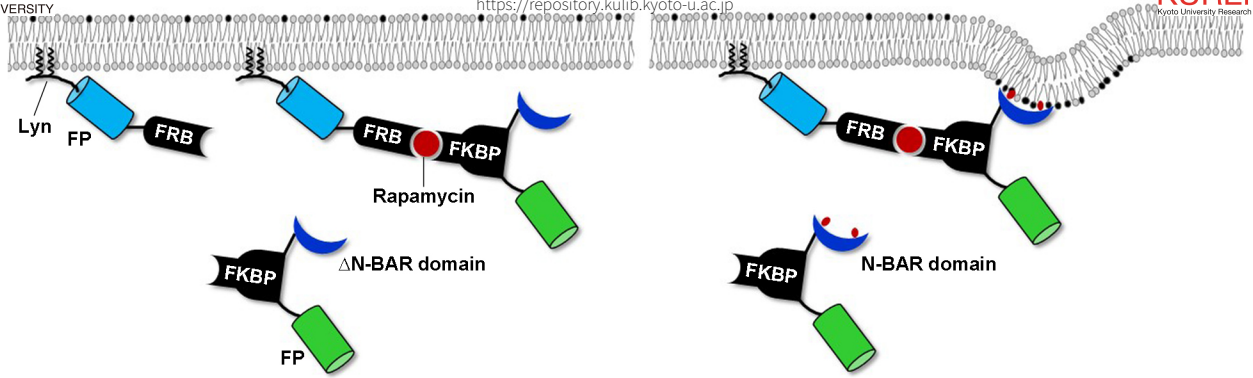
Figure EV1 Takada et al
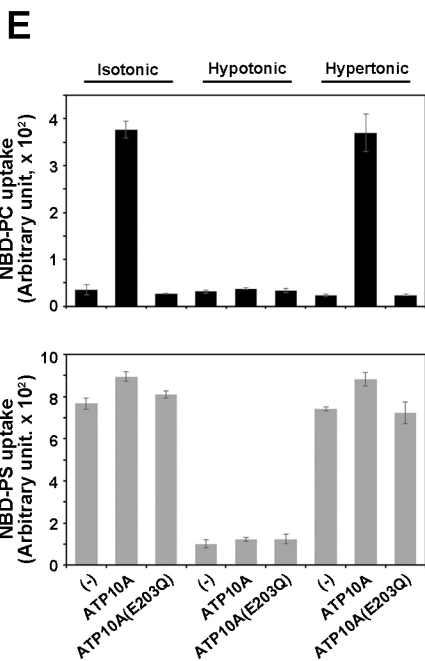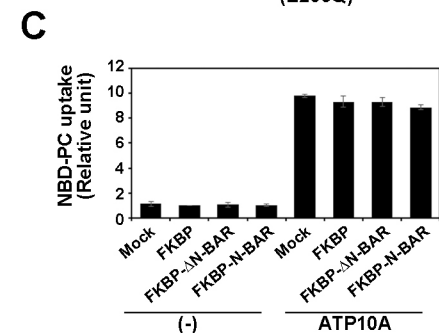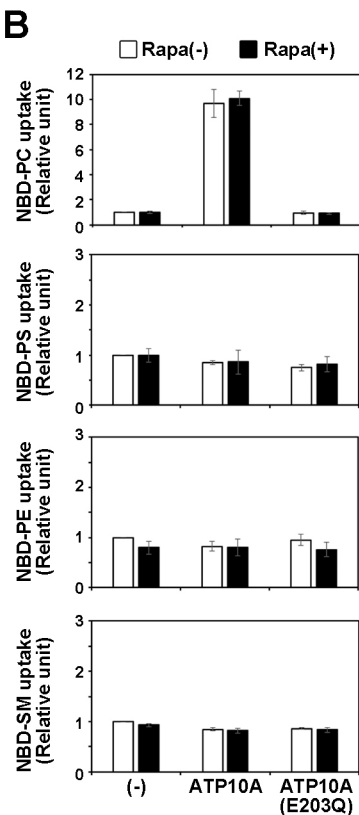
Figure EV2 Takada et al.

**Figure EV3 Takada et al.**
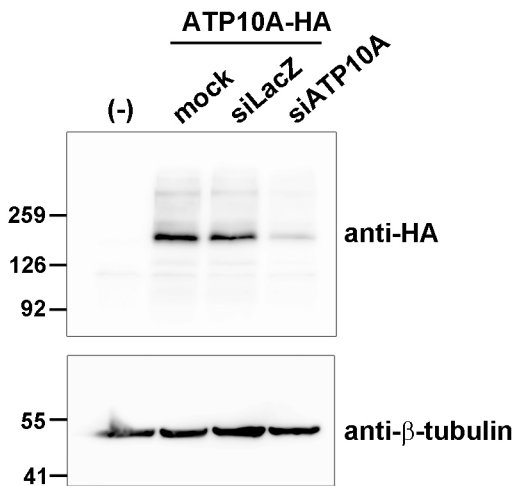
**Figure EV4 Takada et al.**

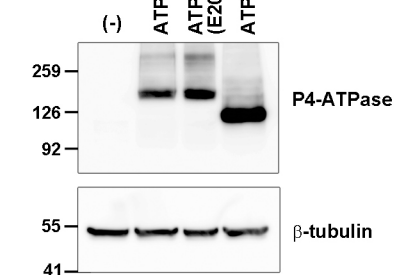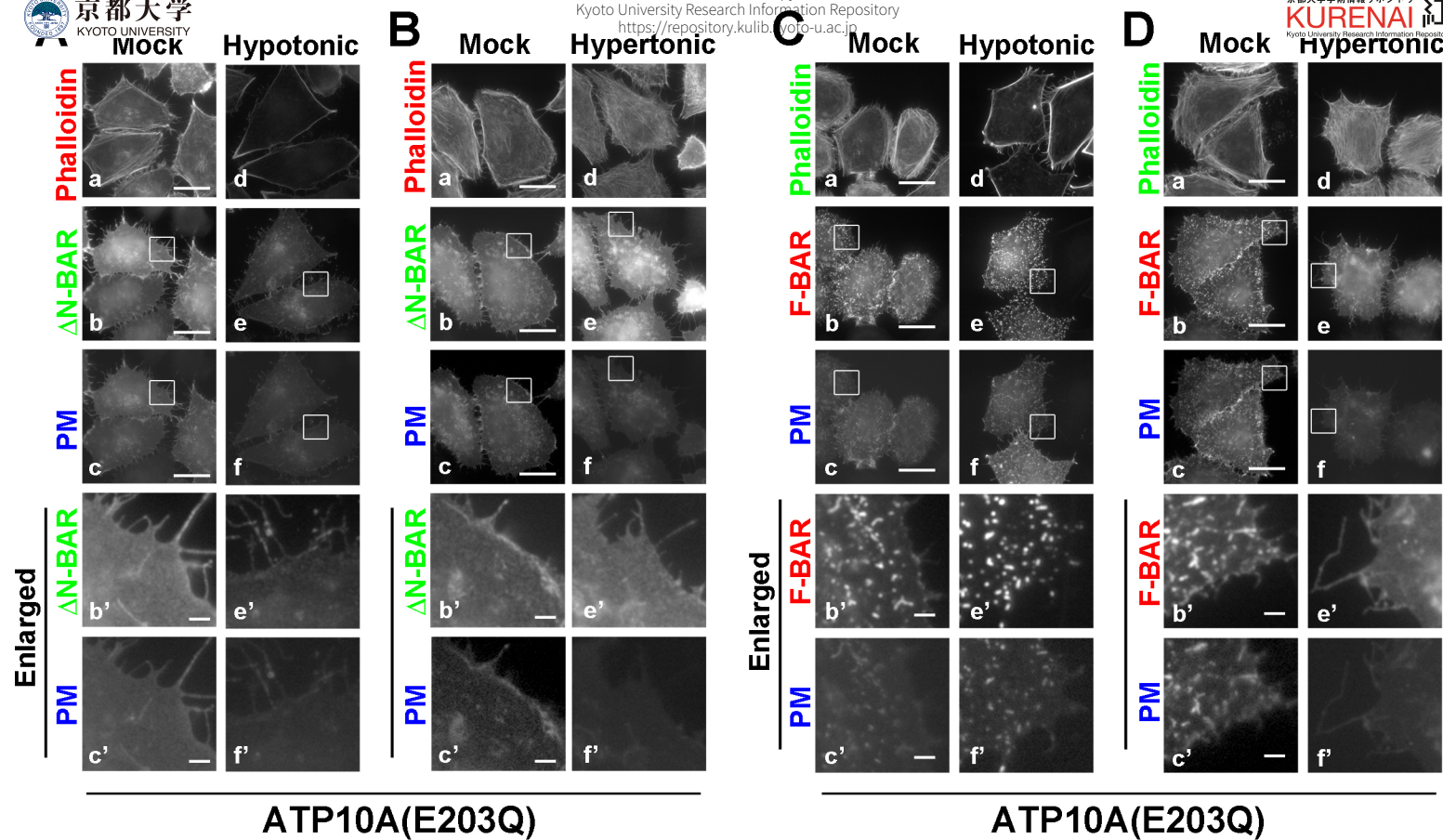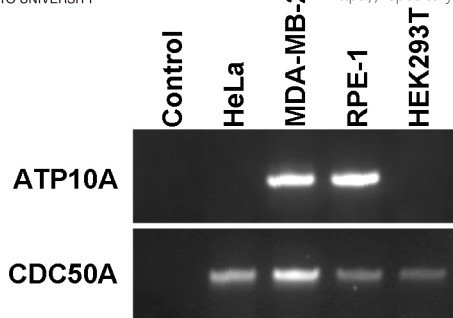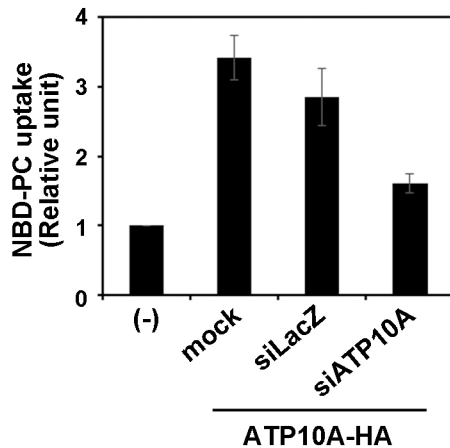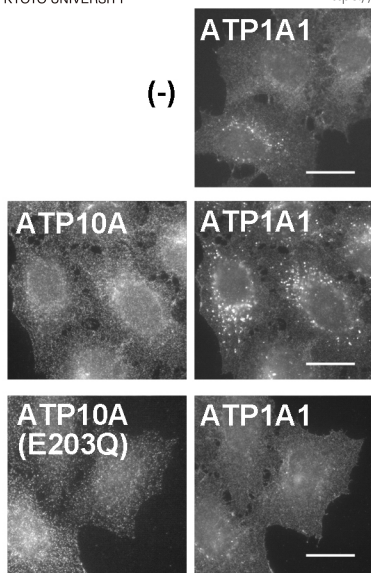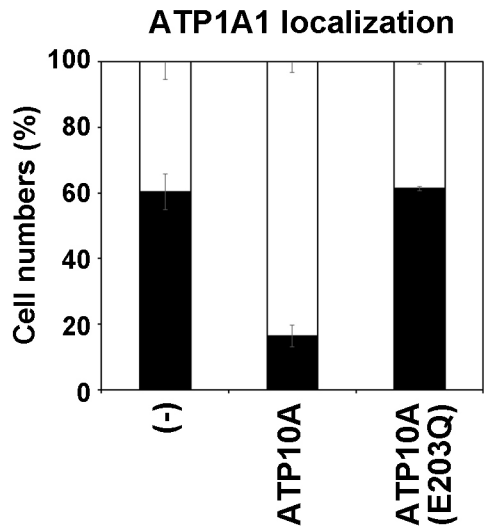**Figure EV5 Takada et al.**

**A**

| P | A | G | T | E | E | P | G | P | P | P | G | R | R | R | R | R | E | G | R | T | R |
|---|---|---|---|---|---|---|---|---|---|---|---|---|---|---|---|---|---|---|---|---|---|
| ccg | gcg | ggg | acc | gag | gag | ccc | ggg | cct | ccg | gga | cgg | cgg | agg | cgc | cga | gag | ggc | agg | acg | cgc | |

10 ... 20

31
| L | L | P | P | P | G | A | E | D | P | A | A | G | A | A | K | G | E | R | R | R | R |
|---|---|---|---|---|---|---|---|---|---|---|---|---|---|---|---|---|---|---|---|---|---|
| ctg | ctg | ccg | ccc | ccg | ggc | gcc | gag | gac | cct | gcg | gct | ggc | gcg | gcc | aag | ggc | gag | cgg | cga | cgg | cgg | cgc | ...... |

40 ... 50

#2 sgRNA target
PAM

#1 sgRNA target
PAM

**B**

clone 1-1

40
| P | A | A | G | A | A | K | G | E | R | R | **R** | **G** | | **R** | **stop** |
|---|---|---|---|---|---|---|---|---|---|---|---|---|---|---|---|
| cct | gcg | gct | ggc | gcg | gcc | aag | ggc | gag | cgg | cg**c** | **ggc** | ........... | **cgg** | **tga** |

50          102

→ 1 base deleted

51
| R | R | R |
|---|---|---|
| ........... **cca ccg** | cgg | cgg | cgc |

donor vector inserted (reverse) ←

clone 2-1

10 ... 20 ...
| E | P | G | P | P | G | R | R | R | R | R | E | G | R | T | R | T | **P** | | **R** | **stop** |
|---|---|---|---|---|---|---|---|---|---|---|---|---|---|---|---|---|---|---|---|---|
| gag | ccc | ggg | cct | ccg | gga | cgg | cgg | agg | cgc | cga | gag | ggc | agg | acg | cgc | acg | **ccg** | ........... | **cgg** | **tga** |

92

→ 31 bases deleted

10 ... 20
| E | P | G | P | P | G | R | R | R | R | R | E | G | R | T | R | T | V | **P** |
|---|---|---|---|---|---|---|---|---|---|---|---|---|---|---|---|---|---|---|
| gag | ccc | ggg | cct | ccg | gga | cgg | cgg | agg | cgc | cga | gag | ggc | agg | acg | cgc | acg | gtg | c**cc** | **tgg** ............ |

→ donor vector inserted (forward)

clone 2-6

31 ... 102
| L | L | P | P | P | G | **P** | | **R** | **stop** |
|---|---|---|---|---|---|---|---|---|---|
| ctg | ctg | ccg | ccc | ccg | gg**g** | **ccg** | ........... | **cgg** | **tga** |

→ 1 base deleted

31
| L | L | P | P | P | G | **P** |
|---|---|---|---|---|---|---|
| ctg | ctg | ccg | ccc | cc**c** | **ggg** | **ccc** | **tgg** ............ |

3 bases inserted
→ donor vector inserted (forward)

**C**

30 min

Intracellular β1-integrin (relative unit)

(−)   clone 1-1   clone 2-1   clone 2-6

ATP10A-KO

**D**

MDA-MB-231 | RPE-1 | Control | MDA-MB-231 | RPE-1 | Control

ATP8B1        ATP8B2

**Figure EV6 Takada et al.**

京都大学
KYOTO UNIVERSITY

京都大学学術情報リポジトリ
KURENAI 紅
Kyoto University Research Information Repository

Treatment (s)

| | Treatment (s) |
| --- | --- |
| Rapa ↓ 0 ──── Fix 15 min | rapamycin |
| Noz ↓ 0 ──── Rapa + Noz ↓ 45 ── Fix 60 min | rapamycin + nocodazole |
| Rapa + Hypo ↓ 0 ──── Fix 15 min | rapamycin + hypotonic stress |
| Rapa + Hyper ↓ 0 ──── Fix 20 min | rapamycin + hypertonic stress |

**Table EV Takada et al.**